USCIPI Report 590

UNIVERSITY OF SOUTHERN CALIFORNIA

STATISTICAL SCENE ANALYSIS: BOUNDARY ESTIMATION OF OBJECTS IN PRESENCE OF NOISE

by

Mohammad H. Jahanshahi

August 1975

Image Processing Institute
University of Southern California
University Park
Los Angeles, California 90007

Sponsored by
Advanced Research Projects Agency
Contract No. F08606-72-C-0008
ARPA Order No. 1706

IPI

IMAGE PROCESSING INSTITUTE

STATISTICAL SCENE ANALYSIS: BOUNDARY ESTIMATION OF OBJECTS IN PRESENCE OF NOISE

by

Mohammad H. Jahanshahi

August 1975

Image Processing Institute
University of Southern California
University Park
Los Angeles, California 90007

This research was supported by the Advanced Research Projects Agency of the Department of Defense and was monitored by the Air Force Eastern Test Range under Contract No. F08606-72-C-0008, ARPA Order No. 1706.

UNCLASSIFIED

Security Classification

DOCUMENT CONTROL DATA - R & D

(Security classification of title, body of abstract and indexing annotation must be entered when the overall report is classified)

1. ORIGINATING ACTIVITY (Corporate author)
Image Processing Institute
University of Southern California, University Park
Los Angeles, California 90007

2a. REPORT SECURITY CLASSIFICATION
UNCLASSIFIED

2b. GROUP

3. REPORT TITLE
STATISTICAL SCENE ANALYSIS:
BOUNDARY ESTIMATION OF OBJECTS IN PRESENCE OF NOISE

4. DESCRIPTIVE NOTES (Type of report and inclusive dates)
Technical Report, August 1975

5. AUTHOR(S) (First name, middle initial, last name)
Mohammad H. Jahanshahi

6. REPORT DATE
August 1975

7a. TOTAL NO. OF PAGES
93

7b. NO. OF REFS
27

8a. CONTRACT OR GRANT NO.
F08606-72-C-0008
ARPA Order [redacted]-1706

9a. ORIGINATOR'S REPORT NUMBER(S)
USCIPI [redacted]-590

9b. OTHER REPORT NO(S) (Any other numbers that may be assigned this report)

10. DISTRIBUTION STATEMENT
Approved for release: distribution unlimited

11. SUPPLEMENTARY NOTES

12. SPONSORING MILITARY ACTIVITY
Advanced Research Project Agency
1400 Wilson Boulevard
Arlington, Virginia 22209

13. ABSTRACT

Automatic computer determination of object boundaries has attracted many researchers in the various areas of image processing for some time. The concept of boundary determination is basically motivated by problems in textural analysis (a subject in scene analysis) and robotics (a subject in artificial intelligence).

In this dissertation, an object boundary estimator, applicable to a class of noisy images, will be introduced. The images considered will contain an object of interest within the background. The boundary estimator will be designed based on the existing estimation techniques through certain available statistics of the object, background, noise, and the boundary. Extensions of the estimator to multi-object images will be discussed as well. The procedures developed will be recursive and readily implementable on a digital computer. A few examples will be considered to illustrate the performance of the estimator.

****

14. Key Words: Scene Analysis, Boundary Estimation, Image Characteristic Function, Replacement Processing.

391 141

DD FORM 1 NOV 68 1473

UNCLASSIFIED

Security Classification

To my Father

ACKNOWLEDGMENT

I wish to thank Professor Nasser E. Nahi, Chairman of my dissertation committee, for his endless patience and encouragements throughout the course of preparing this dissertation. His superb personality and strong character are without parallel in the opinion of this student.

I wish to, further, thank the other members of my dissertation committee, Professors Leonard M. Silverman and J. Pierce, for their contributions to my research.

My appreciation is also extended to Professor W. K. Pratt and the staff of the Image Processing Institute for their support given in preparation of this work.

My special thanks go to my wife Valerie for her years of patience, understanding and encouragement.

Last, but not least, I would like to thank my fellow graduate students F. Davarian, F. Naderi, M. Naraghi, and J. Payrovian for making my years at USC most enjoyable.

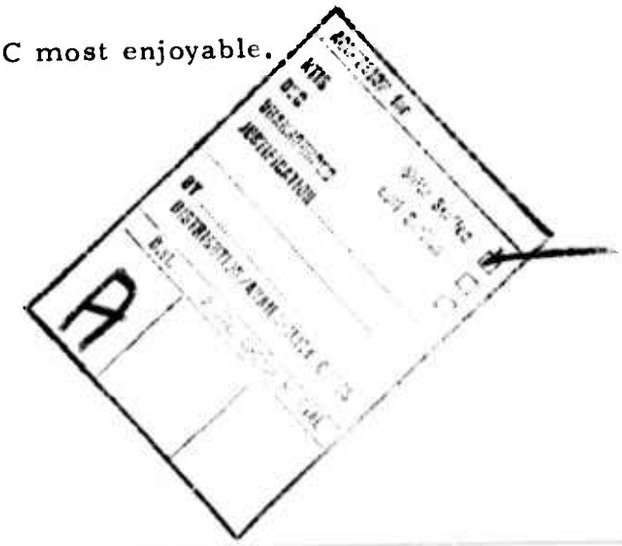

ABSTRACT

Automatic computer determination of object boundaries has attracted many researchers in the various areas of image processing for some time. The concept of boundary determination is basically motivated by problems in textural analysis (a subject in scene analysis) and robotics (a subject in artificial intelligence).

In this dissertation, an object boundary estimator, applicable to a class of noisy images, will be introduced. The images considered will contain an object of interest within the background. The boundary estimator will be designed based on the existing estimation techniques through certain available statistics of the object, background, noise, and the boundary. Extensions of the estimator to multi-object images will be discussed as well. The procedures developed will be recursive and readily implementable on a digital computer. A few examples will be considered to illustrate the performance of the estimator.

TABLE OF CONTENTS

TABLE OF CONTENTS (Cont'd)

Chapter 1

INTRODUCTION

In visual perception, among the most effective stimulus configurations are the "edges" outlining the objects within an image, [1,2]. This has motivated many researchers in the areas of automated image processing, specifically those in scene analysis, to develop various techniques of edge detection and boundary determination.

An incentive for research in scene analysis is the study of robotics, [3]. The available information about the shapes and sizes of physical objects constitute the total visual intelligence required by a robot. Such informations can be provided through knowledge of object boundaries.

Defining the set of points which separate the object and background as "object boundary," the purpose of this report is to develop a recursive, easily implementable, estimator to yield an estimate of the object boundary.

In preparation toward that goal, a survey of the existing boundary determination techniques is made in Chapter II. It will be shown that present techniques are generally based on image models representing overall image brightness functions. An image model, labeled as the "replacement processing," will be defined which considers not only the intensity details of the image, but also explicitly contains

the boundary information within the image.

In Chapter III, the replacement processing model will be utilized to formulate a boundary estimator for a certain class of images. The images considered will contain an object of interest within a background. The boundary estimator will be designed based on a combination of deterministic and probabilistic information pertaining to the image.

Chapter IV will be concerned with the development of possible solutions resulting in an implementable boundary estimator. Recursiveness of the estimator will be our prime objective. A number of examples will be provided to demonstrate the applicability of the boundary estimator.

In Chapter V, an analysis of the boundary estimator, regarding its performance, will be undertaken. Extensions of the estimator to multiobject images will be considered, and, areas with potential for future research will be explored.

Chapter II

STATE OF THE ART: PAST AND PRESENT

A digital image is commonly represented by a two dimensional discrete function, b(m, n), whose range is the grey level values of the image and whose domain spans the entire image.

In general, as a deterministic function, the image function b(m, n) does not carry any salient properties common to all images other than the constraints imposed on it by image recording and/or displaying systems. Examples of such constraints are positiveness and boundedness of b(m, n). Statistical representations of images are, hence, in order.

Statistical image models are generally based on the knowledge of the mean and autocorrelation functions of b(m, n). It has been shown, [4], that two dimensional, wide sense stationary random processes, possessing exponential autocorrelation functions of the form

$$Eb(m_1, n_1)b(m_2, n_2) = \mu e^{-\alpha|m_2-m_1|-\beta|n_2-n_1|},$$

represent suitable models for b(m, n). The justification is basically experimental. Such statistical models have been previously used in image restoration and enhancement problems, [5-7]. However, consistant in the results has been the presence of blurry edges. Intuitively, we may conclude, an image model based solely on the

first two moments of b(m, n) might be suitable for reconstruction of image grey level values, but it does not carry sufficient information to adequately reconstruct the object boundary. This conclusion has been our main motivation in the development of a boundary estimator. A boundary estimator, combined with the image estimators introduced in [5] and [7], would result in an improved restoration of the image.

Along the way, we became aware of the importance of boundary estimators in other areas of automated image processing such as scene analysis and artificial intelligence.

Before proceeding any further, a brief review of existing methods in edge detection and boundary determination is in order. For this purpose, we have relied extensively on References [8] and [9], because of their elaborate coverage of the subject. An attempt has been made, however, to provide the reader with a complete list of relevant bibliography at the end of this report.

In the following sections (2.1-2.6), a description of the basic techniques regarding boundary determination is delineated. The list of bibliography is intended to be complementary to the material covered, and those not covered for the sake of brevity, in this chapter.

2.1 Thresholding

Thresholding is the simplest method of data extraction. Basically, the image function b(m, n), representing the intensity (grey level) values of the image, is compared with two threshold values, T_1 and

T_2. If $T_1 \leq b(m,n) \leq T_2$, the grey level value corresponding to $b(m,n)$ is set to some preselected constant, $\bar{b}$. Otherwise, it is set to zero. The thresholds T_1 and T_2 can be obtained through inspection of the image histogram.

A variation of this technique is to perform thresholding on some transform of $b(m,n)$. High pass filtering of the image function Fourier transform is an example. Since high spatial frequencies of an image correspond to sharp edges, [8], high pass filtering is a technique to extract boundaries.

In general, thresholding is applied along with spatial differencing (described below) to outline objects within an image. Its sensitivity to noise, and the fact that threshold values differ from picture to picture, limit the usage of the technique.

2.2 Spatial Differencing: Noise Free Images

One method of boundary determination is to locate the abrupt dark-light transition regions within an image. In terms of the image function $b(m,n)$, such regions correspond to points in the image where the gradient of $b(m,n)$ retains "large" magnitudes. Here, the term "large" is relative to an arbitrary threshold value.

Different definitions of image gradient have been given in the literature, [8, 10]. The most common is the "Roberts cross operator," $R(m,n)$, defined as

$$(2.2.1) \qquad R(m,n) = \sqrt{[b(m,n)-b(m+1,n+1)]^2+[b(m,n+1)-b(m+1,n)]^2}.$$

If a picture element with grey level value $b(m_0, n_0)$ belongs to an edge, the magnitude of $R(m_0, n_0)$ will be large; whereas, if $b(m_0, n_0)$ belongs to a relatively uniform intensity region, the magnitude of $R(m_0, n_0)$ will be small.

In practice, for computational efficiency, a simplified version of the above operator, namely,

$$F(m,n) = |b(m,n)-b(m+1,n+1)| + |b(m,n+1)-b(m+1,n)| , \tag{2.2.2}$$

is implemented instead. It can be verified by inspection that $F(m,n)$ behaves qualitatively as $R(m,n)$. In fact,

$$R(m,n) \leq F(m,n) \leq \sqrt{2}\, R(m,n) . \tag{2.2.3}$$

The major disadvantages of this technique are again related to the selection of an optimum threshold. If $R(m,n)$, or equivalently $F(m,n)$, is compared to a too large a threshold, some significant edges will be lost. Similarly, a small threshold will cause the appearance of sparious outlines. The existence of noise in the image is another source of restraint in boundary determination through spatial differencing.

2.3 Spatial Differencing: Noisy Images

Different methods for reducing the adverse effects of noise in boundary determination have been suggested in the literature. Typical ones underscore some combination of averaging and differencing of the noisy image function. Denoting such functions by

$$y(m,n) = b(m,n) + v(m,n), \tag{2.3.1}$$

where v(m, n) represents the noise function, an operator frequently suggested is

$$D(m,n) = \left| \frac{1}{A_{w_1}} \sum_{w_1(m,n)} \sum y(i,j) - \frac{1}{A_{w_2}} \sum_{w_2(m,n)} \sum y(i,j) \right|. \tag{2.3.2}$$

The parameters used to define this operator are $w_1(m,n)$ and $w_2(m,n)$, representing two arbitrary contiguous regions in the image with areas A_{w_1} and A_{w_2}, respectively. Comparing D(m, n) to a preselected threshold, then, will constitute whether the picture element b(m, n) belongs to an edge.

Choosing appropriate region sizes for w_1 and w_2 is an important factor in construction of this operator. If regions w_1 and w_2 are chosen too large, a blurring of the edge position will result. Too small regions, on the other hand, could introduce sparious boundary points.

An ingenious, however ad-hoc, modification of the above operator has been presented in [11]. Specifically, let

$$d_k(m,n) = \left| \frac{1}{A_{w_1}(k)} \sum_{w_1(m,n;k)} \sum y(i,j) - \frac{1}{A_{w_2}(k)} \sum_{w_2(m,n;k)} \sum y(i,j) \right|, \tag{2.3.3}$$

where $k = 1, 2, 4, 8, \ldots, 2^{\ell}$, with ℓ being a non-negative integer number. To explain the notation, we resort to equation (2.3.2). For each value of k, $w_1(m,n;k)$ represents a subregion in the image such that

$$\bigcup_{k=1}^{2^{\ell}} w_1(m,n;k) = w_1(m,n) , \tag{2.3.4}$$

where $\cup$ denotes the union of sets. Similarly for $w_2(m,n;k)$,

$$\bigcup_{k=1}^{2^{\ell}} w_2(m,n;k) = w_2(m,n) . \tag{2.3.5}$$

Variables $A_{w_1}(k)$ and $A_{w_2}(k)$ represent the areas associated with subregions $w_1(m,n;k)$ and $w_2(m,n;k)$, respectively. The modified operator is, then, defined as

$$\overline{D}(m,n) = d_1(m,n)d_2(m,n)\ldots d_{2^{\ell}}(m,n) . \tag{2.3.6}$$

This operator has been shown (experimentally) to perform superior to $D(m,n)$, [11, 12]. Its implementation, however, requires selection of optimum region sizes (value of ℓ) and threshold which, as far as fully automated boundary determination techniques are concerned, makes it wanting.

2.4 Spatial Differentiation: High Order Derivatives

In a rigorous mathematical setting, the gradient of a two dimensional function $b(m,n)$ is defined as follows. Let $b(x,y)$ denote the continuous version of the discrete image function $b(m,n)$. Then, the directional derivative of $b(x,y)$, at a point (x_0, y_0), is defined as

$$\left.\frac{\partial b}{\partial \theta}\right|_{(x_0,y_0)} = b_x(x_0,y_0)\cos\theta + b_y(x_0,y_0)\sin\theta , \tag{2.4.1}$$

where θ represents a specified direction relative to the orthogonal x-y coordinate system, and

$$b_x(x_0, y_0) = \left.\frac{\partial b(x, y)}{\partial x}\right|_{(x_0, y_0)} \tag{2.4.2}$$

$$b_y(x_0, y_0) = \left.\frac{\partial b(x, y)}{\partial y}\right|_{(x_0, y_0)} \tag{2.4.3}$$

The gradient, $\nabla b(x, y)$, of the function $b(x, y)$ is, then, a vector originating from point (x_0, y_0), pointing in the direction in which $b(x, y)$ has its maximum directional derivative. Its magnitude is given by

$$|\nabla b(x_0, y_0)| = \sqrt{b_x^2(x_0, y_0) + b_y^2(x_0, y_0)}\ , \tag{2.4.4}$$

[13].

In terms of the digital image function $b(m, n)$, the partial derivative functions $b_x(x, y)$ and $b_y(x, y)$ can be approximated by

$$b_x(x, y) \approx b(m, n+1) - b(m, n) \tag{2.4.5}$$

$$b_y(x, y) \approx b(m+1, n) - b(m, n)\ , \tag{2.4.6}$$

or, alternatively,

$$b_x(x, y) \approx b(m, n) - b(m+1, n+1) \tag{2.4.7}$$

$$b_y(x, y) \approx b(m, n+1) - b(m+1, n)\ , \tag{2.4.8}$$

depending on the orientation of the orthogonal x-y coordinate system.

Replacing for (2.4.5) and (2.4.6) into (2.4.4), yields

$$(2.4.9)\quad |\nabla b(x,y)| \approx \sqrt{[b(m,n+1)-b(m,n)]^2+[b(m+1,n)-b(m,n)]^2} \ .$$

or, replacing for (2.4.7) and (2.4.8) into (2.4.4), we obtain

$$(2.4.10)\quad |\nabla b(x,y)| \approx \sqrt{[b(m,n)-b(m+1,n+1)]^2+[b(m,n+1)-b(m+1,n)]^2} \ .$$

Comparing (2.4.10) with (2.2.1), one concludes

$$(2.4.11)\qquad R(m,n) \approx |\nabla b(x,y)| \ .$$

Thus, as expected, "Roberts cross operator" is an approximation to the actual gradient of the continuous image function b(x, y)

In the same manner as above, higher order derivatives of b(x, y) can be approximated to represent spatial differentiation operators utilized in boundary determination. For example, the "Laplacian operator," L(m, n), defined as

$$(2.4.12)\quad L(m,n) = |b(m,n+2)-2b(m,n+1)+2b(m,n) - 2b(m+1,n)+b(m+2,n)| \ ,$$

is an approximation of

$$(2.4.13)\qquad |\nabla^2 b(x,y)| = |b_{xx}(x,y)+b_{yy}(x,y)| \ ,$$

where b_{xx} and b_{yy} denote the second partial derivatives of the continuous image function b(x, y).

"Bi-Laplacian operator," an approximated version of

$$(2.4.14) \quad \nabla^4 b(x,y) = b_{xxxx}(x,y) + 2b_{xx}(x,y)b_{yy}(x,y) + b_{yyyy}(x,y) ,$$

is another variation of the operators employed for boundary determination.

In general, an operator with higher order derivatives utilizes a larger region of the image to decide on the position of the picture element represented by b(m, n). A Laplacian operator, for instance, employs five picture elements (see Fig. II.1), namely b(m, n), b(m, n+1), b(m, n+2), b(m+1, n), and b(m+2, n), as opposed to the gradient operator (equation (2.4.9)) which employs three picture elements in determining whether b(m, n) is an edge point.

Other operators, based on approximation of image function partial derivatives, have been proposed in the literature, [10]. The quality of the processed pictures, however, are about the same, because basic disadvantages connected with spatial differencing techniques, mentioned in the foregoing sections, are persistantly present irrespective of the choice of the operator.

2.5 Contour Following

Contour following is a heuristic recursive algorithm for boundary determination. Different contour following routines have been proposed by several authors, [14-18]. Sophistication of these routines are based on the complexity and contents of the images under consideration.

m, n	m, n+1	m, n+2
m+1, n	m+1, n+1	m+1, n+2
m+2, n	m+2, n+1	m+2, n+2

Figure II. 1. Image Elements Used to Define Gradient Operator and Laplacian Operator

In the simplest case, namely that of binary images, the contour following procedure is described as follows. Starting at a pre-selected location, one scans the image until an object element is identified. The scanner is, then, moved to the left of its current position to the next picture element. If the new location is an object element, the scanner is turned left again. Otherwise, it is moved toward the right. This procedure is continued until the scanner returns to within one picture element of its initial position. Figure II.2 illustrates the above operation for the case of a two-level image. The image consists of a white diamond-shaped object within a dark background.

Although contour following algorithms are simple to implement, because of their serial nature, they are very sensitive to positioning errors. For example, if a mistake is made in the identity of a picture element (whether it belongs to the background or object), total loss of a portion of the boundary could occur. Creation of sparious edges is another result of wrongfully identifying an image element.

Based on the above analysis, contour following techniques are restricted to noise free or, at best, low noise images. Special purpose contour following algorithms have been developed which sacrifice simplicity for better performance by considerably increasing the amount of computation time, [14-18].

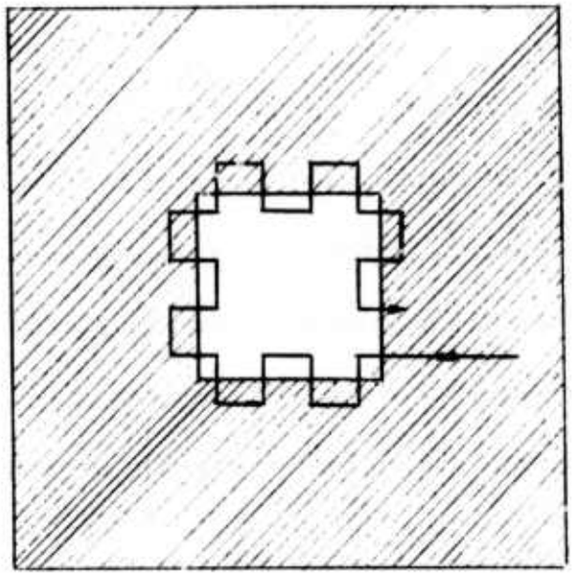

Figure II.2. Boundary Determination by Contour Following. Connected Lines Describe the Object. Arrowed Line Traces the Square Object.

2.6 Statistical Differencing

Let $\bar{b}(m,n)$ be obtained through averaging of the image function $b(m,n)$ over a region w in the image. Furthermore, let

$$\sigma(m,n) = \left\{ \sum_{w(m,n)} \sum [b(i,j)-\bar{b}]^2 \right\}^{\frac{1}{2}} \tag{2.6.1}$$

Then, method of "statistical differencing," [19], utilizes an operator $T(m,n)$, of the form

$$T(m,n) = \frac{b(m,n) - \bar{b}(m,n)}{\sigma(m,n)} , \tag{2.6.2}$$

To determine whether the picture element $b(m,n)$ belongs to an edge location or not. Note, $\sigma^2(m,n)$ defines the variance of the grey level values, $b(m,n)$, over the region $w(m,n)$. The reason for explicitly denoting $\bar{b}$ and σ in terms of m and n is to emphasize their dependence on the selected region size.

This method is specially attractive for detection of minor edges in an image. An example should illustrate this feature more clearly.

Let us select a rectangular region of grid size 3 by 4 within an image (see Figure II.3). The region is constructed so as to represent a minor edge, i.e., the grey level value differences at edge points, $\Delta b(m,n)$, are small. Refering to Figure II.3, definition of $\bar{b}$, and equation (2.6.1), the following values for $\bar{b}$ and σ are obtained.

$$\bar{b} = 1.05 \tag{2.6.3}$$

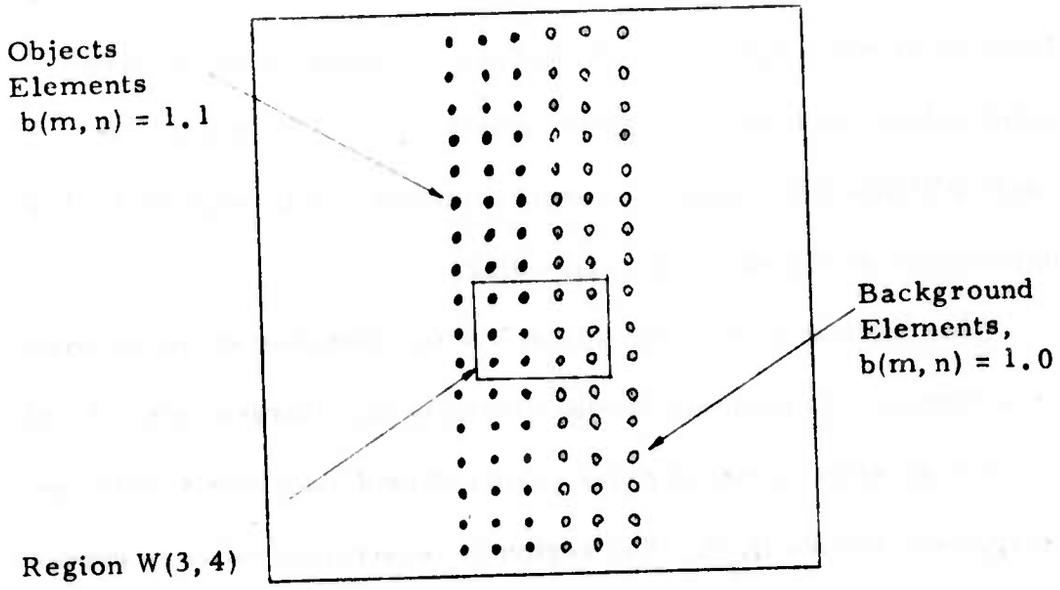

Figure II.3. Binary Image With a Minor Edge, ($\Delta b = .1$).

(2.6.4) $$\sigma = .17$$

(2.6.5) $$T = \begin{cases} -.3 & \text{in the background} \\ +.3 & \text{in the object .} \end{cases}$$

Replacing values of b(m, n) with T(m, n). The minor edge becomes six times more conspicuous ($\Delta T(m, n) = .6$ as opposed to $\Delta b(m, n) = .1$).

Method of statistical differencing, therefore, is suitable for extracting boundary out of images with a lot of detail. By its nature, however, this technique is restricted to noise free images.

2.7 Replacement Processes

Having covered the basic past techniques of boundary determination, the ground work for the introduction of a new technique, described in Chapter III, is developed here.

A mathematical model for the image function b(m, n) which explicitly considers the object boundaries along with image internal details is proposed as follows. Let

(2.7.1) $$\Gamma = \{\gamma_i\}_{i=0}^{N}$$

Represent a sequence of nonnegative, integer, and binary valued functions such that

(2.7.2) $$\sum_{i=0}^{N} \gamma_i = 1$$

(2.7.3) $$\prod_{i=j}^{N} \gamma_i = 0, \quad j = 0, 1, \ldots, N-1 .$$

Relationships (2.7.2) and (2.7.3) restrict the elements of Γ to be all zero with the exception of only one element (any element) whose value must be 1. The image function is now represented by

$$b(m,n) = \sum_{i=0}^{N} \gamma_i(m,n) b_i(m,n) \tag{2.7.4}$$

where the functions $b_i(m,n)$, $0 \le i \le N$, denote the grey level values of the background (i=0) and the N objects in the image. The elements of the sequence Γ carry the boundary information of the objects within the image.

The two dimensional functions $b_0, b_1, \ldots, b_N$ are assumed to be sample functions of N+1 statistically independent, wide sense stationary random processes whose first two moments are known. The two moments, namely the mean and autocorrelation functions, are respectively indicative of the brightness and textural similarities of $b_0, b_1, \ldots, b_N$. Note, an autocorrelation function with a sharp drop off from its maximum corresponds to a finely textured region of the image, [20].

The binary valued function $\gamma_i(m,n)$, another random process, takes values of 1 or zero corresponding to points in the image belonging to the $i^{\underline{th}}$ object or the $j^{\underline{th}}$ $(j \neq i)$ object, respectively. In the literature, this function is usually labeled as the image "characteristic function," [19]. The statistical properties of γ_i will be described later as the need arises.

The image model (2.7.4) is based on a concept defined as "replacement processing," where, by definition, a segment of a function or random process is replaced by another function or random process according to certain rule. Considering that for typical images the object signals, in fact, "replace" a portion of the background signal, and/or each others (as in the cases of overlapping objects), the structure of this model is justified. In model (2.7.4), the replacement takes place according to the values of $\gamma_i(m, n)$. For example, for a non-overlapping $3^{\underline{rd}}$ object, the replacement of the background signal by the object signal occurs within the portion of the image where $\gamma_3(m, n) = 1$.

For future reference, note that the domains of the sample functions $b_0(m, n), \ldots, b_N(m, n)$ are defined to be the entire image. This, in fact, is the main motivation behind introducing the concept of replacement processing in image modeling. Figures II.4 and II.5 illustrate a few examples of constructing an image by replacement processing.

In practice, the grey level values of an image, b(m, n), here after referred to as "original image," are not available for measurement. In lieu of the original image, a sequence of variables, y(m, n), approximating b(m, n) are available for observation. This is due to the existance of disturbances such as reflections from spurious objects, inaccuracies in the image sensing mechanism, corruption

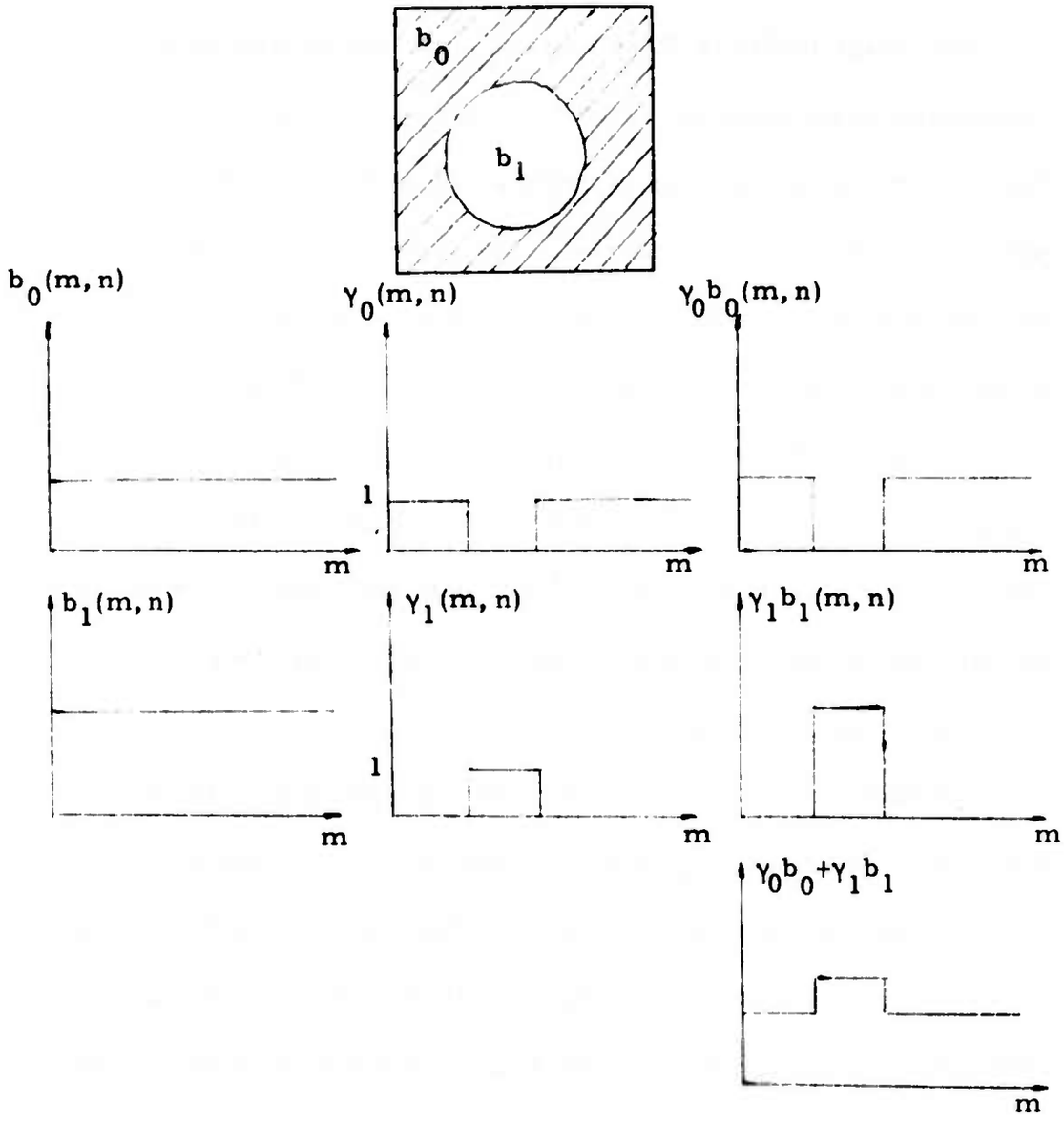

Figure II.4. Construction of a Uniform, Two-Level, Single-Object Image. Cross Section of a Typical Line n is Shown.

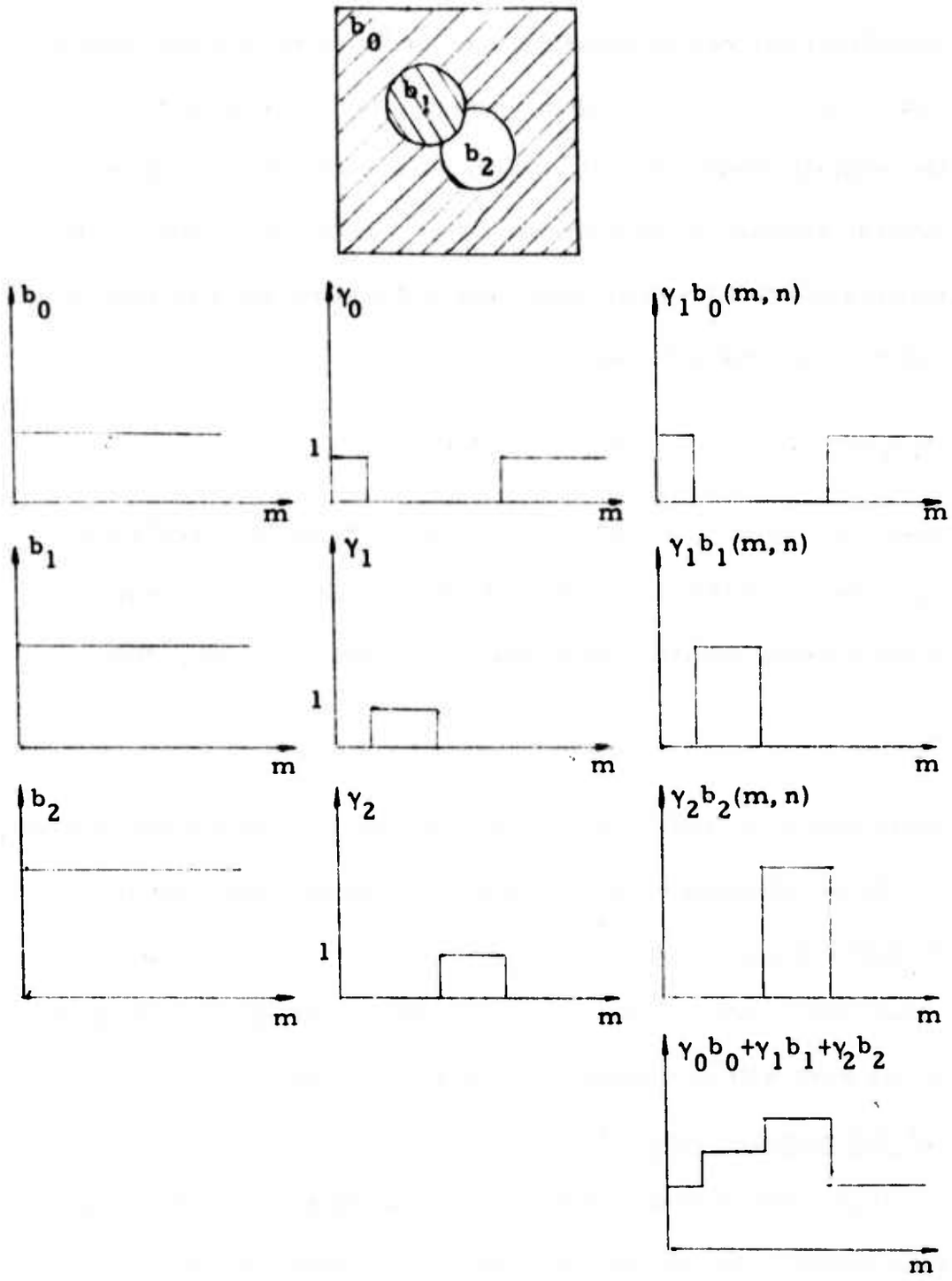

Figure II.5. Construction of a Uniform, Three-Level, Two-Object (Overlapping) Image. Cross Section of a Typical Line n is Shown.

introduced during transmission, film grain noise, and etc. which cause distortion of the original image. The relationship between the original image, b(m, n), and the observable image, y(m, n), depends directly on the sources of degradation. For instance, distortions due to film grain noise, generally introduce a multiplicative noise on the original image; i.e.,

$$y(m,n) = b(m,n)v(m,n) \quad , \tag{2.7.5}$$

where v(m, n) is a random process representing the degradation phenomena. In this work, we will consider the more common types of distortions, namely, those modeled by additive noise. Hence,

$$y(m,n) = b(m,n) + v(m,n) \quad , \tag{2.7.6}$$

where b(m, n) is defined in (2.7.4), and v(m, n) is as delineated above.

In the following chapter, a specific case of image modeling through replacement processing will be used to estimate object boundaries. Prior to that, however, the type of objects considered in this work will be described in the next section.

2.8 Horizontally Convex Objects

In general, boundary determination techniques which incorporate some geometrical properties of the objects within the image into their algorithm are superior to others, [10]. Connectivity and convexity are typical examples of such geometrical features. In this work, we will consider images which contain "horizontally convex"

objects. An object is defined to be horizontally convex if the set forming that object can be characterized as follows.

Definition: A set $E \subset \mathbb{R}^2$ is said to be "horizontally convex" if given $\underline{x}^1 = (x_1^1, x_2^1) \in E$, $\underline{x}^2 = (x_1^2, x_2^2) \in E$, with $x_1^1 \neq x_1^2$ and $x_2^1 = x_2^2$, then $\alpha \underline{x}^1 + (1-\alpha)\underline{x}^2 \in E$, where $0 < \alpha < 1$.

Examples of such sets are E_1 and E_2 in Figures II.6a and II.6b, respectively. Set E_3 (Fig. II.6c) is not horizontally convex.

Note that "horizontal convexity" is a less restrictive condition than "convexity." In other words, a convex set is always horizontally convex, but a horizontally convex set is not necessarily convex. This fact can be observed in Fig. II.6a-II.6c.

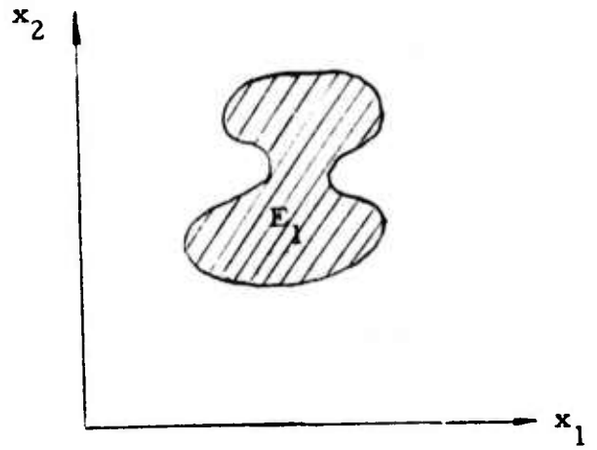

Figure II. 6a. Example of a Horizontally Convex Set.

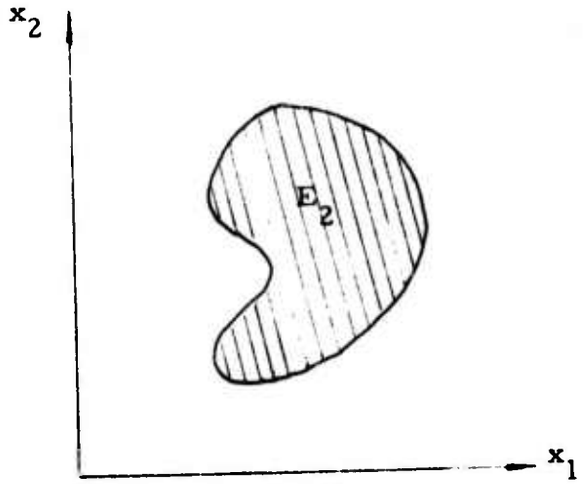

Figure II. 6b. Example of a Horizontally Convex Set.

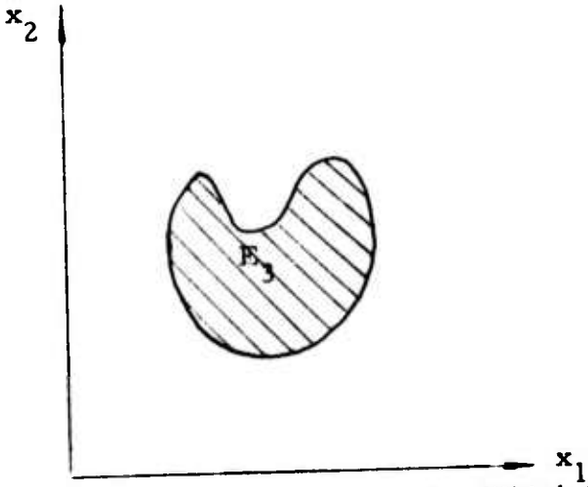

Figure II. 6c. Example of a Set Which is Not Horizontally Convex.

Chapter III

ESTIMATION OF OBJECT BOUNDARY: FORMULATION

In this chapter, we will develop a boundary estimator for a certain class of noisy images. The images belonging to this class can be partitioned into two regions: background and foreground. The foreground forms a horizontally convex object. An object of interest will always be assumed to exist in the image. Techniques developed in [21] may be used to detect the existence of the object in cases when its presence is not certain. The concept of replacement processing, described in Chapter II, and the mathematical image model associated with it, defined by relationship (2.7.4), will be utilized here to formulate the boundary estimation problem.

3.1 Modeling

A model for a single object image whose grey level values are represented by the two dimensional discrete function b(m, n) is defined as

$$b(m,n) = \gamma(m,n)b_0(m,n) + [1-\gamma(m,n)]\,b_b(m,n). \tag{3.1.1}$$

This model is based on the replacement processing concept delineated in section 2.7. The two dimensional functions $b_0(m,n)$ and $b_b(m,n)$ represent intensity level values of the object and the background, respectively, and $\gamma(m,n)$ carries the boundary infor.ma-

tion of the object within the image. Object and background functions, $b_0(m,n)$ and $b_b(m,n)$, are assumed to be sample functions of two statistically independent, wide sense stationary random processes whose first two moments are given. The mean values of b_0 and b_b are indications of the object and background brightness similarities, whereas, their respective autocorrelation functions are measures of the object and background textural information. The binary valued function $\gamma(m,n)$, another random process, takes values of 1 or 0 corresponding to the points in the image belonging to the object or the background respectively. The statistical properties of γ will be described shortly. Note, the characteristic functions $\gamma(m,n)$ and $[1-\gamma(m,n)]$ satisfy relationships (2.7.2) and (2.7.3). Furthermore, note that (3.1.1) is compatible with the image model (2.7.4) for $N = 1$. Hence, (3.1.1) is a replacement processing model for the image signal $b(m,n)$, and, as a result, the domain of the sample functions $b_0(m,n)$ and $b_b(m,n)$ are the entire image.

A sequence of observations constructed as

$$y(m,n) = b(m,n) + v(m,n) \tag{3.1.2}$$

are assumed available for measurement, where $b(m,n)$ is as defined in (3.1.1), and $v(m,n)$ denotes an uncorrelated process representing the observation noise.

3.2 Scanning

An image scanner is now employed to transform the planar data representing the noisy image, $y(m,n)$, into temporal data, $y(k)$. The scanner output, in the absence of observation noise, is denoted by $s(k)$, where

$$s(k) = \lambda(k)s_0(k) + [1-\lambda(k)]\, s_b(k) \tag{3.2.1}$$

models the image in terms of its grey level values and object boundary as viewed by the output of a line by line scanner.

The structure of the one dimensional model (3.2.1) preserves the replacement processing concept. The functions $s_0(k)$ and $s_b(k)$ are associated with $b_0(m,n)$ and $b_b(m,n)$, respectively. In other words, $s_0(k)$ and $s_b(k)$ denote the intensity values of the scanned object and background, and are assumed to be sample functions of two statistically independent, cyclo-stationary random processes, [5, 22], whose first two moments are obtainable directly in terms of the first and second order statistics of $b_0(m,n)$ and $b_b(m,n)$, [23]. As in the case of b_0 and b_b, the domain of the sample functions $s_0(k)$ and $s_b(k)$ are the entire scanned image.

The binary valued function $\lambda(k)$ is the one dimensional counterpart of $\gamma(m,n)$. Its statistics are described in section 3.3. Note that the statistics of $\lambda(k)$ completely define those of $\gamma(m,n)$.

The two dimensional observation sequence $y(m,n)$ in (3.1.2) will also be replaced by its scanned version defined as

$$y(k) = s(k) + v(k) , \tag{3.2.2}$$

where s(k) is as defined in (3.2.1), and v(k) is a zero mean Gaussian white noise process with variance σ^2.

3.3 Representation of $\lambda(k)$

Let m_1 and m_2 denote the first and the last lines of the object as viewed by the scanner. Furthermore, let α_ℓ and β_ℓ represent the beginning and end points of the object on line ℓ, respectively. In general, m_1, m_2, α_ℓ, and β_ℓ, for $m_1 \le \ell \le m_2$, are random.

The function $\lambda(k)$, appearing in (3.2.1), is now defined in terms of m_1, m_2, α_ℓ, and β_ℓ as

$$\lambda(k) = \sum_{\ell=m_1}^{m_2} u[k-\alpha_\ell-(\ell-1)J] - u[k-\beta_\ell-(\ell-1)J] , \tag{3.3.1}$$

where $u[\cdot]$ is the unit step function, J denotes the number of picture elements in one line of the image, and $\beta_\ell \ge \alpha_\ell$. The statistics of the process $\lambda(k)$ can now be given in terms of the statistics of m_1, m_2, and

$$w_\ell = (\alpha_\ell, \beta_\ell) . \tag{3.3.2}$$

Let us assume w_ℓ to form a first order Markov process. This assumption is made for the sake of computational simplicity, and it emphasizes the dependence of the object boundary points on line ℓ upon the boundary points located on the previous line, ℓ-1. It is further assumed that the density functions $p(\alpha_\ell | \alpha_{\ell-1}, \beta_{\ell-1}, m)$,

$p(\beta_\ell | \alpha_\ell, \alpha_{\ell-1}, \beta_{\ell-1}, m_1)$, $p(m_2|m_1)$, and $p(m_1)$ are given, and that

$$(3.3.3) \qquad p(w_\ell | w_{\ell-1}, m_1, m_2) = p(w_\ell | w_{\ell-1}, m_1) .$$

For future reference, notice

$$(3.3.4) \qquad p(w_\ell | w_{\ell-1}, m_1) = p(\alpha_\ell, \beta_\ell | \alpha_{\ell-1}, \beta_{\ell-1}, m_1)$$

$$(3.3.5) \qquad p(\alpha_\ell, \beta_\ell | \alpha_{\ell-1}, \beta_{\ell-1}, m_1) = p(\alpha_\ell | \alpha_{\ell-1}, \beta_{\ell-1}, m_1) \cdot p(\beta_\ell | \alpha_\ell, \alpha_{\ell-1}, \beta_{\ell-1}, m_1) ;$$

therefore,

$$(3.3.6) \quad p(w_\ell | w_{\ell-1}, m_1) = p(\alpha_\ell | \alpha_{\ell-1}, \beta_{\ell-1}, m_1) p(\beta_\ell | \alpha_\ell, \alpha_{\ell-1}, \beta_{\ell-1}, m_1).$$

3.4 Problem Statement

Relationships (3.2.1), (3.2.2), and (3.3.1) along with the definitions and assumptions given in the previous section 3.3, constitute the basis for the boundary estimation problem of this chapter. The objective here is to locate the object boundary. For this purpose, estimates of the first and last lines (m_1 and m_2), and estimates of the starting and ending points (α_ℓ and β_ℓ) of the object are sought. Looked upon as an estimation problem, the problem statement is summarized as follows. Define

$$(3.4.1) \qquad s(k) = \lambda(k) s_0(k) + [1-\lambda(k)] s_b(k)$$

$$(3.4.2) \qquad y(k) = s(k) + v(k)$$

$$(3.4.3) \qquad \lambda(k) = \sum_{\ell = m_1}^{m_2} u[k-\alpha_\ell - (\ell-1)J] + u[k-\beta_\ell - (\ell-1)J] ,$$

where,

i) $Es_0(k)$, $Es_0(k_1)s_0(k_2)$, $Es_b(k)$, and $Es_b(k_1)s_b(k_2)$ are given;

ii) $w_\ell = (\alpha_\ell, \beta_\ell)$ represents a first order Markov sequence for $m_1 \leq \ell \leq m_2$;

iii) $\beta_\ell \geq \alpha_\ell$ for $m_1 \leq \ell \leq m_2$;

and iv) $p(\alpha_\ell | \alpha_{\ell-1}, \beta_{\ell-1}, m_1)$, $p(\beta_\ell | \alpha_\ell, \alpha_{\ell-1}, \beta_{\ell-1}, m_1)$, $p(m_2 | m_1)$, and $p(m_1)$ are known.

Then we wish to obtain a set of estimates for m_1, m_2, α_ℓ, and β_ℓ, $m_1 \leq \ell \leq m_2$, based on the available observation sequence, $y(k)$, $1 \leq k \leq N$. The fixed integer N denotes the total number of picture elements in the image.

3.5 Grey Level Value Estimates

The boundary estimation procedure developed in this chapter, as it will be shown, requires the values of $s_0(k)$ and $s_b(k)$, $1 \leq k \leq N$. Since, in general, these values are not known (cases of known images are exceptional), a set of estimates of $s_0(k)$ and $s_b(k)$, often minimum mean square estimates, will be used in their place. Based on the given mean and autocorrelation functions of $s_0(k)$ and $s_b(k)$, a set of minimum mean square estimates of $s_0(k)$ and $s_b(k)$ can be obtained by implementation of the results in [23]. Note that the concept of replacement processing assures the existance of the estimates of $s_0(k)$ and $s_b(k)$ for <u>all</u> k in the range of $[1, N]$. Since the aim of this dissertation is estimation of object boundary, throughout this

chapter, we will assume the values of $s_0(k)$ and $s_b(k)$, or their corresponding minimum mean square estimates, are given.

3.6 Boundary Points Estimates

The boundary estimation problem, as is evident from (3.4.1) and (3.4.2), is a nonlinear estimation problem. Moreover, due to the type of nonlinearities involves (such as the binary nature of $\lambda(k)$), the available estimators based on linearization concepts (such as extended Kalman-Bucy filters) do not yield satisfactory results. In the sequel, a set of maximum a-posteriori (MAP) estimates for the unknowns m_1, m_2, α_ℓ, and β_ℓ, $m_1 \leq \ell \leq m_2$, are obtained.

Consider an image of grid size M by J, resulting in a total of N pixels (picture elements). The fixed integers M and J denote the number of lines in the image and the total number of pixels in each line of the image, respectively. Let us define

$$\underline{m} = (m_1, m_2) \tag{3.6.1}$$

$$\underline{W} = (w_{m_1}, w_{m_1+1}, \ldots, w_{m_2}) \tag{3.6.2}$$

where w_ℓ, $m_1 \leq \ell \leq m_2$, is defined in (3.3.2). The objective in this section is to derive the MAP estimates of $\underline{m}$ and $\underline{W}$.

Consider relationship (3.4.2) as the observation model. Define the M-dimensional vectors S, Y, and V as

$$S(\underline{m}, \underline{W}) = [\mathscr{s}_1, \mathscr{s}_2, \ldots, \mathscr{s}_M]' \tag{3.6.3}$$

(3.6.4) $$Y = [Y_1, Y_2, \ldots, Y_M]'$$

(3.6.5) $$V = [V_1, V_2, \ldots, V_M]'$$

where "prime" denotes transposition, and

(3.6.6) $$\mathcal{S}_\ell = \begin{cases} [s_b[(\ell-1)J+1], s_b[(\ell-1)J+2], \ldots, s_b[\ell J]]' \text{ for } & 1 \le \ell < m_1 \\ & m_2 < \ell \le M \\ [s_b[(\ell-1)J+1], \ldots, s_b[(\ell-1)J+\alpha_\ell - 1], s_0[(\ell-1)J+\alpha_\ell], \ldots, & \\ s_0[(\ell-1)J+\beta_\ell], s_b[(\ell-1)J+\beta_\ell+1], \ldots, s_b[\ell J]]' \text{ for } m_1 \le \ell \le m_2 & \end{cases}$$

(3.6.7) $$Y_\ell = [y[(\ell-1)J+1], y[(\ell-1)J+2], \ldots, y[\ell J]]', \quad 1 \le \ell \le M$$

(3.6.8) $$V_\ell = [v[(\ell-1)J+1], v[(\ell-1)J+2], \ldots, v[\ell J]]', \quad 1 \le \ell \le M$$

are each a vector of dimension J. Then, from (3.4.2),

(3.6.9) $$Y = S(\underline{m}, \underline{W}) + V$$

where Y is the observation vector. The observation noise, V, is assumed a Gaussian process with mean zero and covariance $\sigma^2 I$, "I" denoting the identity matrix.

The form of the vector $S(\underline{m}, \underline{W})$, defined by (3.6.3) and (3.6.6) is a consequence of having one object of interest. The reason for explicitly denoting S in terms of $\underline{m}$ and $\underline{W}$ is to underscore the variables we are specifically concerned with. Note that the vector S is random due to the randomness of $\underline{m}$ and $\underline{W}$, or equivalently m_1, m_2, α_ℓ, and β_ℓ, $m_1 \le \ell \le m_2$.

To proceed with the MAP estimation of $\underline{m}$ and $\underline{W}$, certain a-priori

statistics are required. The given density functions $p(m_1)$, $p(m_2|m_1)$, $p(\alpha_\ell|\alpha_{\ell-1}, \beta_{\ell-1}, m_1)$, and $p(\beta_\ell|\alpha_\ell, \alpha_{\ell-1}, \beta_{\ell-1}, \cdots m_1)$ will be shown to suffice.

It is well known that MAP estimates of $\underline{m}$ and $\underline{W}$ are such values of $\underline{m}$ and $\underline{W}$ that maximize the joint probability density function $p(Y, \underline{m}, \underline{W})$, where Y, $\underline{m}$, and $\underline{W}$ are as defined in (3.6.9), (3.6.1), and (3.6.2), respectively, [24]. From (3.6.9), where V was assumed Gaussian with mean zero and variance σ^2, and based on the fact that

$$p(Y, \underline{m}, \underline{W}) = p(Y|\underline{m}, \underline{W})p(\underline{W}|\underline{m})p(\underline{m}) \tag{3.6.10}$$

we have

$$p(Y, \underline{m}, \underline{W}) = (2\pi\sigma^2)^{-\frac{N}{2}} \exp\left\{ -\frac{1}{2\sigma^2} [Y-S(\underline{m}, \underline{W})]' \cdot [Y-S(\underline{m}, \underline{W})] + \ln p(\underline{W}|\underline{m}) + \ln p(\underline{m}) \right\}. \tag{3.6.11}$$

Taking natural logarithm of both sides of (3.6.11) yields

$$\ln p(Y, \underline{m}, \underline{W}) = -\frac{1}{2\sigma^2} [Y-S(\underline{m}, \underline{W})]'[Y-S(\underline{m}, \underline{W})]' [Y-S(\underline{m}, \underline{W})] + \ln p(\underline{W}|\underline{m}) + \ln p(\underline{m}) \; . \tag{3.6.12}$$

Taking natural logarithm of both sides of (3.6.11) yields

$$\ln p(Y, \underline{m}, \underline{W}) = -\frac{1}{2\sigma^2} [Y-S(\underline{m}, \underline{W})]'[Y-S(\underline{m}, \underline{W})] + \ln p(\underline{W}|\underline{m}) + \ln p(\underline{m}) - \frac{N}{2} \ln 2\pi\sigma^2 \; . \tag{3.6.12}$$

Note that since logarithm is a monotonic function, those values of $\underline{m}$ and $\underline{W}$ which maximize $p(Y, \underline{m}, \underline{W})$ coincide with the mode of

$\ln p(Y, \underline{m}, \underline{W})$. Considering the foregoing comment and the fact that the last term on the right side of (3.6.12) is a constant, maximizing $\ln p(Y, \underline{m}, \underline{W})$ is, then, equivalent to

$$(3.6.13) \qquad \max_{\underline{m}, \underline{W}} \left\{ -\frac{1}{2\sigma^2} [Y - S(\underline{m}, \underline{W})]' [Y - S(\underline{m}, \underline{W})] + \ln p(\underline{W} | \underline{m}) + \ln p(\underline{m}) \right\} .$$

Furthermore, expanding the expression inside braces in (3.6.13), and considering that the term $Y'Y$ is invariant under maximization of $\underline{m}$ and $\underline{W}$, (3.6.13) is equivalent to

$$(3.6.14) \qquad \max_{\underline{m}, \underline{W}} \left\{ -\frac{1}{2\sigma^2} S'(\underline{m}, \underline{W}) [S(\underline{m}, \underline{W}) - 2Y] + \ln p(\underline{W} | \underline{m}) + \ln p(\underline{m}) \right\} .$$

or,

$$(3.6.15) \qquad \min_{\underline{m}, \underline{W}} \{ S'(\underline{m}, \underline{W}) [S(\underline{m}, \underline{W}) - 2Y] - 2\sigma^2 \ln p(\underline{W} | \underline{m}) - 2\sigma^2 \ln p(\underline{m}) \} .$$

Before proceeding with the minimization process in (3.6.15), let us transform it from vector into scalar notation. From (3.6.3) and (3.6.6), we obtain

$$(3.6.16) \qquad S'(\underline{m}, \underline{W}) S(\underline{m}, \underline{W}) = \sum_{\ell=1}^{M} \mathcal{S}_\ell' \mathcal{S}_\ell =$$

$$\sum_{\ell=1}^{m_1 - 1} \sum_{k=(\ell-1)J+1}^{\ell J} s_b^2(k) + \sum_{\ell=m_1}^{m_2} \left[\sum_{k=(\ell-1)J+1}^{(\ell-1)J+\alpha_\ell - 1} s_b^2(k) + \sum_{k=(\ell-1)J+\alpha_\ell}^{(\ell-1)J+\beta_\ell} s_0^2(k) + \sum_{k=(\ell-1)J+\beta_\ell+1}^{\ell J} s_b^2(k) \right] + \sum_{\ell=m_2+1}^{M} \sum_{k=(\ell-1)J+1}^{\ell J} s_b^2(k) .$$

Similarly, from (3.6.3), (3.6.4), (3.6.6), and (3.6.7), we obtain

$$(3.6.17)\quad S'(\underline{m}, \underline{W})Y = \sum_{\ell=1}^{M} \alpha'_\ell Y_\ell =$$

$$\sum_{\ell=1}^{m_1-1} \sum_{k=(\ell-1)J+1}^{\ell J} s_b(k)y(k) + \sum_{\ell=m_1}^{m_2} \left[\sum_{k=(\ell-1)J+1}^{(\ell-1)J+\alpha_\ell-1} s_b(k)y(k) + \right.$$

$$\left. \sum_{k=(\ell-1)J+\alpha_\ell}^{(\ell-1)J+\beta_\ell} s_0(k)y(k) + \sum_{k=(\ell-1)J+\beta_\ell+1}^{\ell J} s_b(k)y(k) \right] +$$

$$\sum_{\ell=m_2+1}^{M} \sum_{k=(\ell-1)J+1}^{\ell J} s_b(k)y(k) \ .$$

Combining (3.6.16) and (3.6.17) results in

$$(3.6.18)\quad S'(\underline{m}, \underline{W})[S(\underline{m}, \underline{W})-2Y] =$$

$$\sum_{\ell=1}^{m_1-1} \sum_{k=(\ell-1)J+1}^{\ell J} K_b(k) + \sum_{\ell=m_1}^{m_2} \left[\sum_{k=(\ell-1)J+1}^{(\ell-1)J+\alpha_\ell-1} K_b(k) + \right.$$

$$\left. \sum_{k=(\ell-1)J+\alpha_\ell}^{(\ell-1)J+\beta_\ell} K_0(k) + \sum_{k=(\ell-1)J+\beta_\ell+1}^{\ell J} K_b(k) \right] + \sum_{\ell=m_2+1}^{M} \sum_{k=(\ell-1)J+1}^{\ell J} K_b(k),$$

where

$$(3.6.19)\quad K_b(k) = s_b(k)[s_b(k)-2y(k)],$$

and

$$(3.6.20)\quad K_0(k) = s_0(k)[s_0(k)-2y(k)]$$

Note that $K_b(k)$ and $K_0(k)$ are defined for all $1 \le k \le N$.

To put (3.6.18) in a more compact form, let us add to and subtract from the right side of (3.6.18) the quantity

$$\sum_{\ell=m_1}^{m_2} \sum_{k=(\ell-1)J+1}^{\ell J} K_b(k).$$

Then (3.6.18) can be written as

$$S'(\underline{m}, \underline{W})[S(\underline{m}, \underline{W})-2Y] = \sum_{\ell=1}^{M} \sum_{k=(\ell-1)J+1}^{\ell J} K_b(k) + \sum_{\ell=1}^{m_2} \sum_{k=(\ell-1)J+\alpha_\ell}^{(\ell-1)J+\beta_\ell} [K_0(k)-K_b(k)]. \tag{3.6.21}$$

Since the first term on the right hand side of (3.6.1), i.e.,

$$\sum_{\ell=1}^{M} \sum_{k=(\ell-1)J+1}^{\ell J} K_b(k) = \sum_{k=1}^{N} K_b(k)$$

is a constant with respect to $\underline{m}$ and $\underline{W}$, it will be omitted out of minimization process (3.6.15). Replacing what is left of (3.6.21) into (3.6.15), we obtain

$$\min_{\underline{m}, \underline{W}} \left\{ -2\sigma^2 \ln p(\underline{m}) - 2\sigma^2 \ln p(\underline{W}|\underline{m}) + \sum_{\ell=m_1}^{m_2} \sum_{k=(\ell-1)J+\alpha_\ell}^{(\ell-1)J+\beta_\ell} [K_0(k)-K_b(k)] \right\}. \tag{3.6.22}$$

Defining

$$K(k) \triangleq K_0(k) - K_b(k) \tag{3.6.23}$$

and

$$T(w_\ell) \triangleq \sum_{k=(\ell-1)J+\alpha_\ell}^{(\ell-1)J+\beta_\ell} K(k) \ , \tag{3.6.24}$$

(3.6.22) can be written as

$$\min_{\underline{m}, \underline{W}} \left\{ -2\sigma^2 \ln p(\underline{m}) - 2\sigma^2 \ln p(\underline{W}|\underline{m}) + \sum_{\ell=m_1}^{m_2} T(w_\ell) \right\} \ . \tag{3.6.25}$$

Furthermore, from (3.3.3), (3.6.2), and the assumption that w_ℓ is first order Markov,

$$p(\underline{W}|\underline{m}) = p(w_{m_2}|w_{m_2-1}, m_1)p(w_{m_2-1}|w_{m_2-2}, m_1) \cdots \tag{3.6.26}$$

$$\cdots p(w_{m_1+1}|w_{m_1}, m_1)p(w_{m_1}|m_1) \ ,$$

where

$$p(w_{m_1}|w_{m_1-1}, m_1) \triangleq p(w_{m_1}|m_1) \ . \tag{3.6.27}$$

From (3.6.26), then,

$$\ln p(\underline{W}|\underline{m}) = \sum_{\ell=m_1}^{m_2} \ln p(w_\ell|w_{\ell-1}, m_1) \ . \tag{3.6.28}$$

Replacing for (3.6.28) and

$$\ln p(\underline{m}) = \ln p(m_1, m_2) = \ln p(m_2|m_1) + \ln p(m_1) \tag{3.6.29}$$

into (3.6.25), yields

$$(3.6.30)\qquad \min_{\underline{m},\,\underline{W}} \left\{ -2\sigma^2 \ln p(m_2|m_1) - 2\sigma^2 \ln p(m_1) + \sum_{\ell=m_1}^{m_2} \left[T(w_\ell) - 2\sigma^2 \ln p(w_\ell|w_{\ell-1}, m_1) \right] \right\} .$$

To obtain MAP estimates of m_1, m_2, α_ℓ, and β_ℓ, $m_1 \le \ell \le m_2$, the minimization in (3.6.30) must be performed. Techniques of finding the extremums of (3.6.30) through differentiation do not apply here since the variables m_1, m_2, α_ℓ, and β_ℓ, $m_1 \le \ell \le m_2$, are not continuous. Alternative methods, however, are possible and will be the subject of the next chapter.

Chapter IV

ESTIMATION OF OBJECT BOUNDARY: PROPOSED SOLUTION

Acquisition of a numerical solution for the minimization process (3.6.30) is an integral part of this dissertation. Since a rigorous solution of (3.6.30), resulting in a set of optimal estimates for m_1, m_2, α_ℓ, and β_ℓ, $m_1 \leq \ell \leq m_2$, is computationally unacceptable, approximate solutions are sought. Two possible approaches, shown later to yield satisfactory results are proposed below.

One approach is to obtain the estimates of α_ℓ and β_ℓ, over the range $m_1 \leq \ell \leq m_2$, with the assumption that values of m_1 and m_2 are given. For example, values of m_1 and m_2 may be chosen as $m_1 = 1$ and $m_2 = M$, implying the object boundary points lie on every line of the image. Then, if necessary, one may utilize additional structural properties of the object to eliminate those boundary points estimates which are incompatible with the given structural information. Examples of structural properties include shape and/or size of the object within the image.

An alternative approach is to consider the problem in two steps; namely, first solve for the estimates of α_ℓ and β_ℓ, $m_1 \leq \ell \leq m_2$, denoted by $\hat{\alpha}_\ell$ and $\hat{\beta}_\ell$, for a selected set of m_1 and m_2. Then, solve for the estimates of m_1 and m_2 ($\hat{m}_1$ and $\hat{m}_2$) by replacing $\hat{\alpha}_\ell$ and $\hat{\beta}_\ell$

for α_ℓ and β_ℓ. A recursive procedure will result if the above two steps are performed at each scan line producing an algorithm which yields a set of estimates for m_1, m_2, α_ℓ, and β_ℓ concurrently.

The former approach, as compared with the latter, is computationally more attractive. However, it requires additional information of a deterministic geometric nature on the object beyond those given statistical information delineated in section 3.4.

We will elaborate on both approaches below.

4.1 Derivation of $\hat{\alpha}_\ell$ and $\hat{\beta}_\ell$ Given m_1 and m_2

In the case when m_1 and m_2 are a-priori given, (3.6.30) can be reduced to

$$(4.1.1) \qquad \min_{\underline{W}} \left\{ \sum_{\ell=m_1}^{m_2} \left[T(w_\ell) - 2\sigma^2 \ln p(w_\ell | w_{\ell-1}, m_1) \right] \right\} .$$

Expanding $p(w_\ell | w_{\ell-1}, m_1)$ as in (3.3.5), (4.1.1) is written as

$$(4.1.2) \qquad \min_{\underline{W}} \left\{ \sum_{\ell=m_1}^{m_2} \left[T(w_\ell) - 2\sigma^2 \ln p(\alpha_\ell | \alpha_{\ell-1}, \beta_{\ell-1}, m_1) - 2\sigma^2 \ln p(\beta_\ell | \alpha_\ell, \alpha_{\ell-1}, \beta_{\ell-1}, m_1) \right] \right\} .$$

Furthermore, from (3.6.24),

$$(4.1.3) \qquad T(w_\ell) = \sum_{k=(\ell-1)J+1}^{(\ell-1)J+\beta_\ell} K(k) - \sum_{k=(\ell-1)J+1}^{(\ell-1)J+\alpha_\ell-1} K(k) .$$

Replacing for $T(w_\ell)$ into (4.1.2) yields

$$(4.1.4)\qquad \min_{\underline{W}} \Bigg\{ \sum_{\ell=m_1}^{m_2} 2\sigma^2 \ln p(\alpha_\ell \mid \alpha_{\ell-1}, \beta_{\ell-1}, m_1) - 2\sigma^2 \ln p(\beta_\ell \mid \alpha_\ell, \alpha_{\ell-1}, \beta_{\ell-1}, m_1) + \sum_{k=(\ell-1)J+1}^{(\ell-1)J+\beta_\ell} K(k) - \sum_{k=(\ell-1)J+1}^{(\ell-1)J+\alpha_\ell-1} K(k) \Bigg\} .$$

A recursive, easily implementable solution of (4.1.4) is possible if the density functions $p(\alpha_\ell \mid \alpha_{\ell-1}, \beta_{\ell-1}, m_1)$ and $p(\beta_\ell \mid \alpha_\ell, \alpha_{\ell-1}, \beta_{\ell-1}, m_1)$ are approximated by $p(\alpha_\ell \mid \hat{\alpha}_{\ell-1}, \hat{\beta}_{\ell-1}, m_1)$ and $p(\beta_\ell \mid \hat{\alpha}_\ell, \hat{\alpha}_{\ell-1}, \hat{\beta}_{\ell-1}, m_1)$, respectively. Hence, the minimization process (4.1.4) is replaced by

$$(4.1.5)\qquad \min_{\underline{W}} \Bigg\{ \sum_{\ell=m_1}^{m_2} [-2\sigma^2 \ln p(\alpha_\ell \mid \hat{\alpha}_{\ell-1}, \hat{\beta}_{\ell-1}, m_1) - 2\sigma^2 \ln p(\beta_\ell \mid \hat{\alpha}_\ell, \hat{\alpha}_{\ell-1}, \hat{\beta}_{\ell-1}, m_1) + \sum_{k=(\ell-1)J+1}^{(\ell-1)J+\beta_\ell} K(k) - \sum_{k=(\ell-1)J+1}^{(\ell-1)J+\alpha_\ell-1} K(k) \Bigg\} .$$

To express (4.1.5) in a compact form, let us define

$$(4.1.6)\qquad g(\alpha_\ell) \triangleq -2\sigma^2 \ln p(\alpha_\ell \mid \hat{\alpha}_{\ell-1}, \hat{\beta}_{\ell-1}, m_1) - \sum_{k=(\ell-1)J+1}^{(\ell-1)J+\alpha_\ell-1} K(k) ,$$

and

$$(4.1.7)\qquad h(\beta_\ell) \triangleq -2\sigma^2 \ln p(\beta_\ell \mid \hat{\alpha}_\ell, \hat{\alpha}_{\ell-1}, \hat{\beta}_{\ell-1}, m_1) + \sum_{k=(\ell-1)J+1}^{(\ell-1)J+\beta_\ell} K(h) ,$$

for $m_1 \le \ell \le m_2$. Then (4.1.5) can be written as

$$\min_{\underline{W}} \left\{ \sum_{\ell=m_1}^{m_2} \left[g(\alpha_\ell) + h(\beta_\ell) \right] \right\} . \tag{4.1.8}$$

Note that, from (3.6.27), for $\ell = m_1$

$$g(\alpha_{m_1}) = -2\sigma^2 \ln p(\alpha_{m_1} | m_1) - \sum_{k=(m_1-1)J+1}^{(m_1-1)J+\alpha_{m_1}-1} K(k) \tag{4.1.9}$$

$$h(\beta_{m_1}) = -2\sigma^2 \ln p(\beta_{m_1} | \hat{\alpha}_{m_1}, m_1) + \sum_{k=(m_1-1)J+1}^{(m_1-1)J+\beta_{m_1}} K(k) . \tag{4.1.10}$$

The minimization process (4.1.8) can now be simplified considerably, because a typical term of the summation in (4.1.8), for example $\ell = m$, is a function of the variables α_m and β_m only. Consequently, (4.1.8) is equivalent to

$$\sum_{\ell=m_1}^{m_2} \min_{\beta_\ell} h(\beta_\ell) + \min_{\alpha_\ell} g(\alpha_\ell) \quad . \tag{4.1.11}$$

This minimization is performed recursively as follows.

Step 1. Determine $\hat{\alpha}_{m_1}$ by minimizing $g(\alpha_{m_1})$. This is possible since, from (4.1.9), $g(\alpha_{m_1})$ is a function of α_{m_1} only.

Step 2. Determine $\hat{\beta}_{m_1}$, based on the result of step 2, by minimizing $h(\beta_{m_1})$. This again is possible since, from (4.1.10), $h(\beta_{m_1})$ is a function of the variables

β_{m_1} and $\hat{\alpha}_{m_1}$ only.

Step 3. Set $\ell = m_1 + 1$.

Step 4. Determine $\hat{\alpha}_\ell$, given $\hat{\alpha}_{\ell-1}$ and $\hat{\beta}_{\ell-1}$ from previous steps, by minimizing $g(\alpha_\ell)$.

Step 5. Determine $\hat{\beta}_\ell$, given $\hat{\alpha}_\ell$, $\hat{\alpha}_{\ell-1}$, and $\hat{\beta}_{\ell-1}$, by minimizing $h(\beta_\ell)$.

Step 6. Set $\ell = \ell + 1$.

Step 7. Check to determine if $\ell > m_2$. If "Yes", go to step 9. If "No", proceed to the next step.

Step 8. Go to step 4.

Step 9. Terminate the computations.

Notice, based on the definition of $\lambda(k)$ in (3.4.3), $\hat{\beta}_\ell$ is constrained to be $\geq \hat{\alpha}_\ell$.

The computational procedure, as described above, is clearly a recursive one. Specific choices of the density functions $p(\alpha_\ell|\hat{\alpha}_{\ell-1}, \hat{\beta}_{\ell-1}, m_1)$ and $p(\beta_\ell|\hat{\alpha}_\ell, \hat{\alpha}_{\ell-1}, \hat{\beta}_{\ell-1}, m_1)$ are required to implement this algorithm. This will be, however, postponed to a later section.

Use of additional structural knowledge about the object (such as its shape) will then complete this approach by locating the actual positions of the first and last lines of the object.

4.2 Derivation of $\hat{m}_1$ and $\hat{m}_2$

We will now elaborate on the second approach referred to before. The first step of the problem, namely that of obtaining $\hat{\alpha}_\ell$ and $\hat{\beta}_\ell$, was

solved in section 4.1. Replacing the estimates $\hat{\alpha}_\ell$ and $\hat{\beta}_\ell$ for α_ℓ and β_ℓ in (3.6.30), reduces the minimization process (3.6.30) to

$$(4.2.1) \qquad \min_{\underline{m}} \left\{ -2\sigma^2 \ln p(m_2|m_1) - 2\sigma^2 \ln p(m_1) + \sum_{\ell=m_1}^{m_2} T(\hat{w}_\ell) \right\} ,$$

where $\hat{w}_\ell = (\hat{\alpha}_\ell, \hat{\beta}_\ell)$, and $T(\hat{w}_\ell)$ is as defined in (3.6.24) with α_ℓ and β_ℓ replaced by $\hat{\alpha}_\ell$ and $\hat{\beta}_\ell$, respectively. Let us define

$$(4.2.2) \qquad \Lambda(m) \triangleq \sum_{\ell=1}^{m} T(\hat{w}_\ell) ;$$

then,

$$(4.2.3) \qquad \Lambda(m_2) - \Lambda(m_1) = \sum_{\ell=m_1}^{m_2} T(\hat{w}_\ell) .$$

Replacing for (4.2.3) into (4.2.1), we obtain

$$(4.2.4) \qquad \min_{\underline{m}} \{ -2\sigma^2 \ln p(m_2|m_1) - 2\sigma^2 \ln p(m_1) + \Lambda(m_2) - \Lambda(m_1 - 1) \} .$$

Considering that $\underline{m} = (m_1, m_2)$, (4.2.4) can be rearranged as follows.

$$(4.2.5) \qquad \min_{m_1} \{ -2\sigma^2 \ln p(m_1) - \Lambda(m_1 - 1) + \min_{m_2} [-2\sigma^2 \ln p(m_2|m_1) + \Lambda(m_2)] \} .$$

Furthermore, let m_1 be uniformly distributed over the discrete interval $[1, M]$; i.e.,

$$(4.2.6) \qquad p(m_1) = \frac{1}{M} ,$$

and let m_2 be uniformly distributed over $[m_1, M]$; i.e.,

$$(4.2.7) \qquad p(m_2|m_1) = \frac{1}{M - m_1} .$$

Then, (4.2.5) can be written as

$$(4.2.8)\quad \min_{m_1} \{2\sigma^2 \ln M - \Lambda(m_1-1) + \min_{m_2} [\, 2\sigma^2 \ln (M-m_1) + \Lambda(m_2)]\}.$$

Crossing out the constant terms and rearranging (4.2.8), yields

$$(4.2.9)\quad \min_{m_1} \{2\sigma^2 \ln (M-m_1) - \Lambda(m_1-1) + \min_{m_2} [\Lambda(m_2)]\}.$$

It is clear that the minimization process (4.2.9), with respect to m_1 and m_2, is separable. That is, it can be considered as two independent extremization processes, namely,

$$(4.2.10)\quad \max_{m_1} [\Lambda(m_1-1) - 2\sigma^2 \ln(M-m_1)], \quad 1 \le m_1 \le M,$$

and

$$(4.2.11)\quad \min_{m_2} [\Lambda(m_2)], \quad m_1 \le m_2 \le M,$$

where satisfying (4.2.10) yields $\hat{m}_1$ and (4.2.11) yields $\hat{m}_2$. In other words, defining

$$(4.2.12)\quad C(m) \triangleq \Lambda(m-1) - 2\sigma^2 \ln (M-m),$$

Estimates of m_1 and m_2 are obtained by locating the relative maximum and minimum of C(m), $1 \le m \le M$, and $\Lambda(m)$, $m_1 \le m \le M$, respectively.

To acquire further insight, variations of $\Lambda(m)$ and C(m) with respect to m are obtained graphically by considering relationship (4.2.2). Noticing that $\Lambda(m)$ is obtained through discrete integration

(summation) of $T(\hat{w}_\ell)$, we will examine this function, i.e., $T(\hat{w}_\ell)$, closely. From (3.6.24),

$$T(\hat{w}_\ell) = \sum_{k=(\ell-1)J+\hat{\alpha}_\ell}^{(\ell-1)J+\hat{\beta}_\ell} K(k) , \tag{4.2.13}$$

or, from (3.6.19), (3.6.20), and (3.6.23),

$$T(\hat{w}_\ell) = \sum_{k=(\ell-1)J+\hat{\alpha}_\ell}^{(\ell-1)J+\hat{\beta}_\ell} s_0(k)[s_0(k)-2y(k)] - s_b(k)[s_b(k)-2y(k)] . \tag{4.2.14}$$

Rearranging the terms in (3.9.14), we obtain

$$T(\hat{w}_\ell) = \sum_{k=(\ell-1)J+\hat{\alpha}_\ell}^{(\ell-1)J+\hat{\beta}_\ell} [s_0(k)-y(k)]^2 - [s_b(k)-y(k)]^2 . \tag{4.2.15}$$

Behavior of Λ in two regions of the image, namely, background and object, are of interest to us. First, let us consider the region of the image corresponding to background. A portion of this region corresponds to where $1 \le \ell \le m_1$ and $m_2 < \ell \le M$, with

$$y(k) = s_b(k) + v(k) . \tag{4.2.16}$$

Replacing for (4.2.16) into (4.2.15), yields

$$T(\hat{w}_\ell) = \sum_{k=(\ell-1)J+\hat{\alpha}_\ell}^{(\ell-1)J+\hat{\beta}_\ell} [s_0(k)-s_b(k)]^2 - 2v(k)[s_0(k)-s_b(k)] . \tag{4.2.17}$$

For the sake of simplicity, let us assume $s_0(k) = \bar{s}_0$ and $s_b(k) = \bar{s}_b$ are constant (case of binary images); then, relationship (4.2.17) reduces to

$$(4.2.18) \qquad T(\hat{w}_\ell) = (\hat{\beta}_\ell - \hat{\alpha}_\ell + 1)(\bar{s}_0 - \bar{s}_b)^2 - 2(\bar{s}_0 - \bar{s}_b) \sum_{k=(\ell-1)J+\hat{\alpha}_\ell}^{(\ell-1)J+\hat{\beta}_\ell} v(k) .$$

Considering that the random process v(k) is zero mean, the summation term in (4.2.18) can be approximated by zero. Therefore,

$$(4.2.19) \qquad T(\hat{w}_\ell) \approx (\hat{\beta}_\ell - \hat{\alpha}_\ell + 1)(\bar{s}_0 - \bar{s}_b)^2 ,$$

for $1 \le \ell < m_1$ and $m_2 < \ell \le M$. Since we restricted $\hat{\beta}_\ell$ to be always $\ge \hat{\alpha}_\ell$, $T(\hat{w}_\ell)$, as represented in (4.2.19), is always a positive quantity. Note the relationship (4.2.19) would be an exact one in cases of noise free binary images.

Now, let us consider the region of the image correponding to the object. A portion of this region is related to where $m_1 \le \ell \le m_2$ with

$$(4.2.20) \qquad y(k) = s_0(k) + v(k) .$$

Similar computations as for the background region results in

$$(4.2.21) \qquad T(\hat{w}_\ell) \approx -(\hat{\beta}_\ell - \hat{\alpha}_\ell + 1)(\bar{s}_0 - \bar{s}_b)^2 ,$$

for $m_1 \le \ell \le m_2$. Relationship (4.2.21) is clearly an indication of $T(\hat{w}_\ell)$ being always a negative quantity in the object region of the image.

From relationships (4.2.19), (4.2.21), and the definition of $\Lambda(m)$ in (4.2.2), we conclude Figures IV.1 and IV.2 represent typical graphs of $\Lambda(m)$.

It is noteworthy to mention that in cases of working with highly degraded images, corresponding to signal-to-noise ratios of less than unity, variations of the form shown in Figure IV.3 have been observed for $\Lambda(m)$. Intuitively, this is due to highly unpredictable oscillatory values introduced by the noise term, $v(k)$, in (4.2.18) as a result of working with low signal-to-noise ratio images. The adverse effect of this problem can be significantly alleviated through inspection of Figures IV.1-IV.3. Notice, the locations of $\hat{m}_1$ and $\hat{m}_2$, in all cases (high or low signal-to-noise ratios), coincide with two significant slope changes in the graphs of $\Lambda(m)$. Therefore, when designing an algorithm to determine those values of m which satisfy criteria (4.2.10) and (4.2.11), we shall exploit this significant-slope-change feature delineated above. Since, as it is evident in Figures IV.1-IV.3, the significant-slope-change feature holds for noise free and low noise images as well as high noise images, the resulting algorithm should be applicable in all cases.

The above artificial manipulation, undertaken to improve the estimates of m_1 and m_2, is analogous to when the optimum Kalman gain of a Kalman-Bucy estimator is varied to improve the resulting estimates. An explicit example of such a situation can be found in [25].

An algorithm has been developed to determine those values of m which maximize $C(m)$ and minimize $\Lambda(m)$ by searching for the

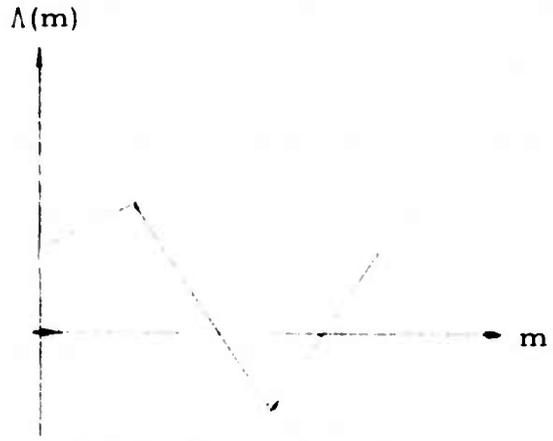

Figure III.1. Noise-Free Image.

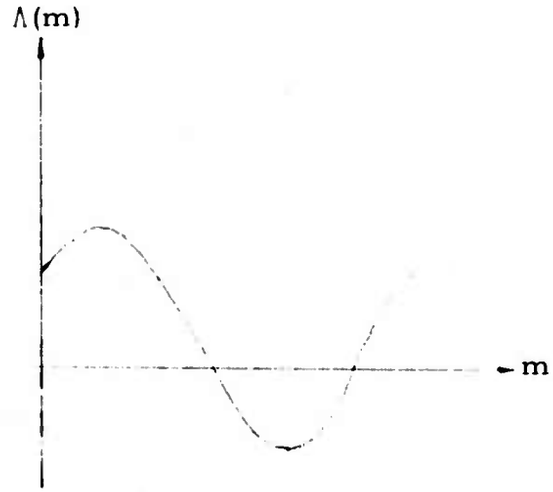

Figure III.2. Noise Image.

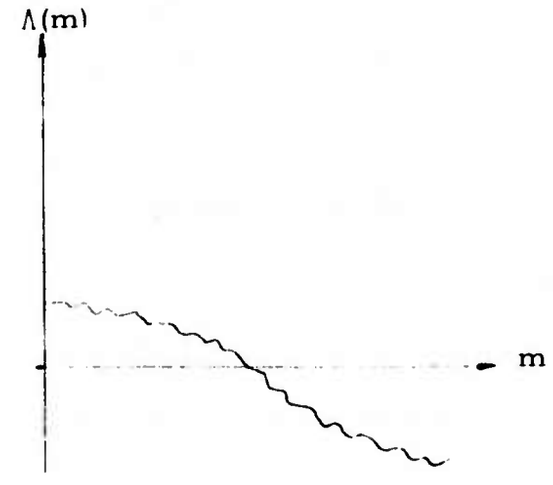

Figure III.3. High-Noise Image.

significant slope changes in C(m) and Λ(m), respectively. Such values of m are accepted as the estimates of first and last lines of the object. Details of this algorithm are best shown concisely by the flow chart in Figure IV.4. The procedure is recursive and easily implementable on a digital computer. Notice that estimates of m_1 and m_2 are computed concurrently with those of α_ℓ and β_ℓ in a line by line manner. Examples in section 4.4 should illustrate the results of this section to our satisfaction.

4.3 Choice of Density Functions for α_ℓ and β_ℓ

To implement the results of section 4.1, specifically to carry out the minimization process of (4.1.11), knowledge of the density functions $p(\alpha_\ell \mid \hat{\alpha}_{\ell-1}, \hat{\beta}_{\ell-1}, m_1)$ and $p(\beta_\ell \mid \hat{\alpha}_\ell, \hat{\alpha}_{\ell-1}, \hat{\beta}_{\ell-1}, m_1)$ are required. Since these functions are to be provided as a part of the given data, two different cases, believed to be typical, will be considered in this work.

First, we will assume the given density functions $p(\alpha_\ell \mid \hat{\alpha}_{\ell-1}, \hat{\beta}_{\ell-1}, m_1)$ and $p(\beta_\ell \mid \hat{\alpha}_\ell, \hat{\alpha}_{\ell-1}, \hat{\beta}_{\ell-1}, m_1)$ describe two normally distributed random variables, α_ℓ and β_ℓ, for all ℓ in the range of $(m_1, m_2]$ except for $\ell = m_1$, i.e., the first line of the object, where α_{m_1} and β_{m_1} are given to be uniformly distributed.

Next, uniform statistics will be assigned to α_ℓ and β_ℓ for all ℓ in the range of $[m_1, m_2]$. In the sequel, a detailed formulation of the results is presented for each case.

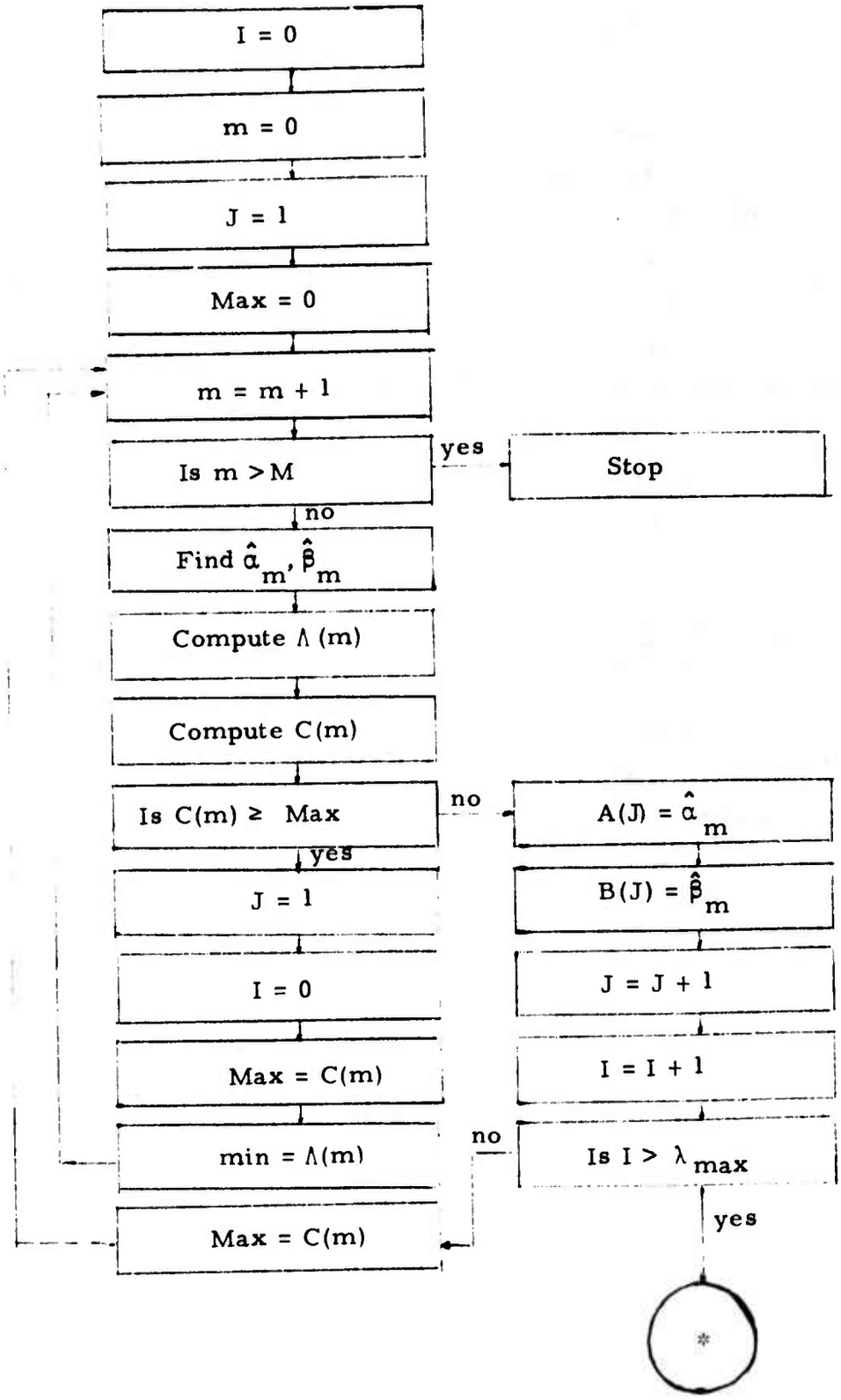

Figure IV.4. Flow Chart For Estimation of Object Boundary.

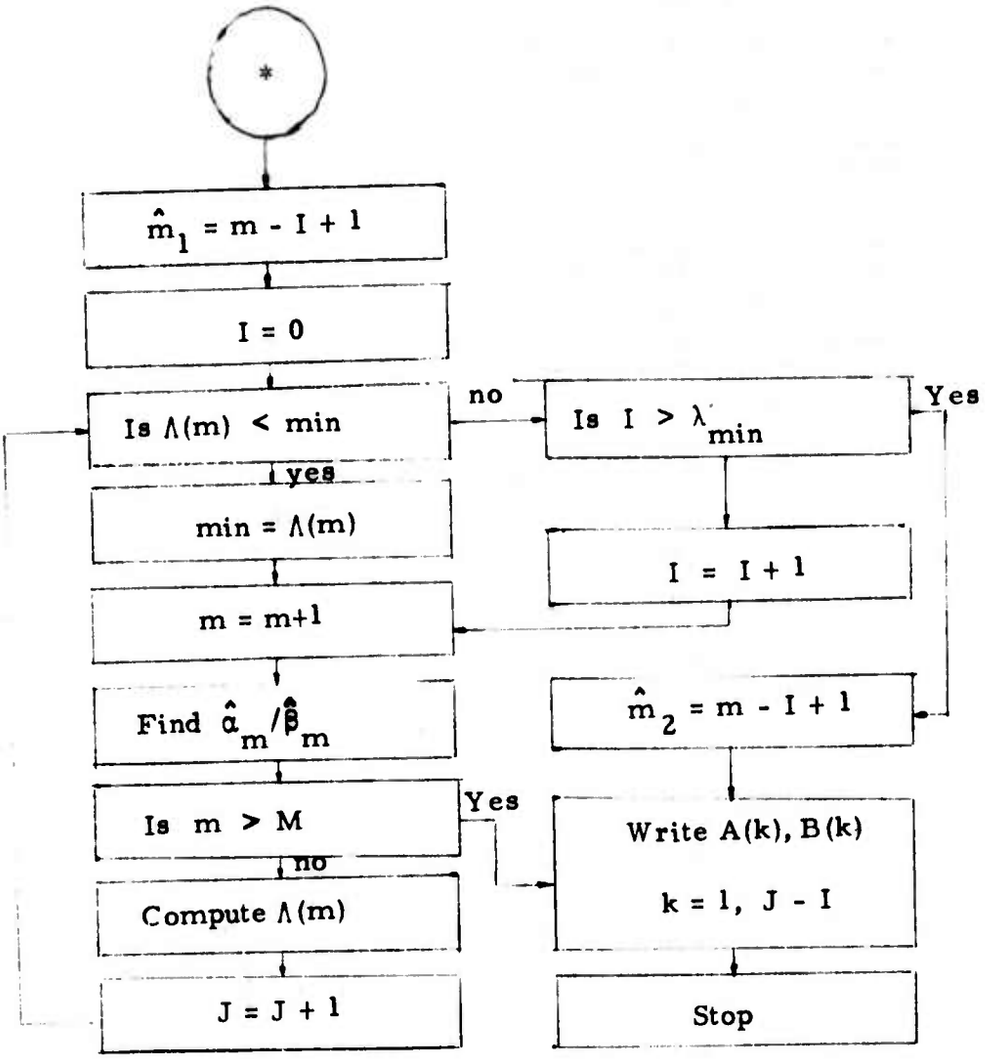

Figure IV.4. Continued.

Since a Gaussian probability density function can be defined completely through the knowledge of first and second order statistics of the random variable, [26], the conditional mean and variance values of α_ℓ and β_ℓ should be sufficient to describe $p(\alpha_\ell | \hat{\alpha}_{\ell-1}, \hat{\beta}_{\ell-1}, m_1)$ and $p(\beta_\ell | \hat{\alpha}_\ell, \hat{\alpha}_{\ell-1}, \hat{\beta}_{\ell-1}, m_1)$ in the Gaussian case. The choices of conditional mean and variance values of α_ℓ and β_ℓ, $m_1+1 \le \ell \le m_2$, are somewhat arbitrary. The motivation behind the values chosen below will be given shortly. Let

$$p(\alpha_{m_1} | m_1) = \frac{1}{J}, \quad 1 \le \alpha_{m_1} \le J, \tag{4.3.1}$$

where J denotes the total number of pixels in every line of the image. Furthermore, for $m_1+1 \le \ell \le m_2$, let

$$E(\alpha_\ell | \hat{\alpha}_{\ell-1}, \hat{\beta}_{\ell-1}, m_1) = \hat{\alpha}_{\ell-1}, \tag{4.3.2}$$

$$\mathrm{Var}(\alpha_\ell | \hat{\alpha}_{\ell-1}, \hat{\beta}_{\ell-1}, m_1) = |\hat{L}_{\ell-1} - L|^2, \tag{4.3.3}$$

where $E(\cdot)$ and $\mathrm{Var}(\cdot)$ denote the mathematical expectation and variance operators, respectively, and

$$\hat{L}_\ell \triangleq \hat{\beta}_\ell - \hat{\alpha}_\ell \tag{4.3.4}$$

$$L \triangleq \max_{m_1 \le \ell \le m_2} (L_\ell) \tag{4.3.5}$$

$$L_\ell \triangleq \beta_\ell - \alpha_\ell . \tag{4.3.6}$$

Similarly for β_ℓ, let

$$(4.3.7)\qquad p(\beta_{m_1} \mid \hat{\alpha}_{m_1}, m_1) = \frac{1}{J-\hat{\alpha}_{m_1}}\ , \quad \hat{\alpha}_{m_1} \le \beta_{m_1} \le J\ ,$$

and, for $m_1+1 \le \ell \le m_2$,

$$(4.3.8)\qquad E(\beta_\ell \mid \hat{\alpha}_\ell, \hat{\alpha}_{\ell-1}, \hat{\beta}_{\ell-1}, m_1) = \hat{\beta}_{\ell-1}$$

$$(4.3.9)\qquad \mathrm{Var}(\beta_\ell \mid \hat{\alpha}_\ell, \hat{\alpha}_{\ell-1}, \hat{\beta}_{\ell-1}, m_1) = |\hat{L}_{\ell-1}-L|^2\ ,$$

where $\hat{L}_\ell$ and L are as defined in (4.3.4) and (4.3.5). From (4.3.2)-(4.3.3) and (4.3.8)-(4.3.9), then,

$$(4.3.10)\qquad p(\alpha_\ell \mid \hat{\alpha}_{\ell-1}, \hat{\beta}_{\ell-1}, m_1) = \frac{1}{\sqrt{2\pi}\,|\hat{L}_{\ell-1}-L|} \exp\left\{-\frac{1}{2|\hat{L}_{\ell-1}-L|^2} \cdot (\alpha_\ell-\hat{\alpha}_{\ell-1})^2\right\}$$

$$(4.3.11)\qquad p(\beta_\ell \mid \hat{\alpha}_\ell, \hat{\alpha}_{\ell-1}, \hat{\beta}_{\ell-1}, m_1) = \frac{1}{\sqrt{2\pi}\,|\hat{L}_{\ell-1}-L|} \exp\left\{-\frac{1}{2|\hat{L}_{\ell-1}-L|^2} \cdot (\beta_\ell-\hat{\beta}_{\ell-1})^2\right\}$$

for $m_1+1 \le \ell \le m_2$ and $\hat{\alpha}_\ell \le \hat{\beta}_\ell \le J$.

In the presence of a finely digitized (sampled) image, [27], it seems reasonable to assume the mean values of α_ℓ and β_ℓ to be at $\alpha_{\ell-1}$ and $\beta_{\ell-1}$ the conditional mean values of α_ℓ and β_ℓ to be at $\hat{\alpha}_{\ell-1}$ and $\hat{\beta}_{\ell-1}$, hence (4.3.2) and (4.3.8).

In choosing the conditional variances of α_ℓ and β_ℓ, the flexibility of the boundary estimator, in the sense of adapting itself to break

away from bad estimates, has been our major concern. It is intuitively desirable to choose the variances of α_ℓ and β_ℓ large when the estimates $\hat{\alpha}_{\ell-1}$ and $\hat{\beta}_{\ell-1}$ are poor and small when they are good. In other words, we would like to encourage the estimator to stay close to $\hat{\alpha}_{\ell-1}$ and $\hat{\beta}_{\ell-1}$ when it is looking for $\hat{\alpha}_\ell$ and $\hat{\beta}_\ell$ only if $\hat{\alpha}_{\ell-1}$ and $\hat{\beta}_{\ell-1}$ are good estimates of $\alpha_{\ell-1}$ and $\beta_{\ell-1}$. The choice of variances as in (4.3.3) and (4.3.9) is an attempt in that direction. Notice the boundary estimator will be less "rigid" in estimating α_ℓ and β_ℓ, if the estimated width of the object on line ℓ-1, i.e., $\hat{L}_{\ell-1}$, is far from the maximum width of the object. The maximum width of the object, L, assumed approximately known in practice, was chosen as an arbitrary reference value.

With density functions $p(\alpha_\ell | \hat{\alpha}_{\ell-1}, \hat{\beta}_{\ell-1}, m_1)$ and $p(\beta_\ell | \hat{\alpha}_\ell, \hat{\alpha}_{\ell-1}, \hat{\beta}_{\ell-1}, m_1)$ given as in (43.1.), (4.3.7), (4.3.10), and (4.3.11), relationships (4.1.6), (4.1.7), (4.1.9), and (4.1.10) can be written as

$$(4.3.12) \qquad g(\alpha_{m_1}) = 2\sigma^2 \ln J - \sum_{k=(m_1-1)J+1}^{(m_1-1)J+\alpha_{m_1}-1} K(k),$$

$$(4.3.13) \qquad g(\alpha_\ell) = \frac{\sigma^2(\alpha_\ell - \hat{\alpha}_{\ell-1})^2}{(\hat{L}_{\ell-1}-L)^2} - \sum_{k=(\ell-1)J+1}^{(\ell-1)J+\alpha_\ell-1} K(k) +$$

$$2\sigma^2 \ln\sqrt{\pi} + \sigma^2 \ln(\hat{L}_{\ell-1}-L)^2$$

$$(4.3.14) \qquad h(\beta_{m_1}) = 2\sigma^2 \ln(J-\hat{\alpha}_{m_1}) + \sum_{k=(m_1-1)J+1}^{(m_1-1)J+\beta_{m_1}} K(k),$$

$$(4.3.15)\qquad h(\beta_\ell) = \frac{\sigma^2(\beta_\ell-\hat{\beta}_{\ell-1})^2}{(\hat{L}_{\ell-1}-L)^2} + \sum_{k=(\ell-1)J+1}^{(\ell-1)J+\beta_\ell} K(k) +$$

$$2\sigma^2 \ln\sqrt{\pi} + \sigma^2 \ln(\hat{L}_{\ell-1}-L)^2 ,$$

where $m_1+1 \le \ell \le m_2$ and $\hat{\alpha}_\ell \le \beta_\ell \le J$ for $m_1 \le \ell \le m_2$. Omitting the constant terms which do not affect the minimization of $g(\alpha_\ell)$ and $h(\beta_\ell)$, we obtain

$$(4.3.16)\qquad g(\alpha_{m_1}) = -\sum_{k=(m_1-1)J+1}^{(m_1-1)J+\alpha_{m_1}-1} K(k) ,$$

$$(4.3.17)\qquad g(\alpha_\ell) = \frac{\sigma^2(\alpha_\ell-\hat{\alpha}_{\ell-1})^2}{(\hat{L}_{\ell-1}-L)^2} - \sum_{k=(\ell-1)J+1}^{(\ell-1)J+\alpha_\ell-1} K(k) + \sigma^2 \ln(\hat{L}_{\ell-1}-L)^2$$

$$(4.3.18)\qquad h(\beta_{m_1}) = \sum_{k=(m_1-1)J+1}^{(m_1-1)J+\beta_{m_1}} K(k) ,$$

$$(4.3.19)\qquad h(\beta_\ell) = \frac{\sigma^2(\beta_\ell-\hat{\beta}_{\ell-1})^2}{(\hat{L}_{\ell-1}-L)^2} + \sum_{k=(\ell-1)J+1}^{(\ell-1)J+\beta_\ell} K(k) + \sigma^2 \ln(\hat{L}_{\ell-1}-L)^2 .$$

Computations of $\hat{\alpha}_\ell$ and $\hat{\beta}_\ell$, $m_1 \le \ell \le m_2$, such that criteria (4.1.11) is satisfied is now routine using equations (4.3.16)-(4.3.19) along with the recursive procedure described in section 4.1.

An alternative choice for the density functions $p(\alpha_\ell|\hat{\alpha}_{\ell-1}, \hat{\beta}_{\ell-1}, m_1)$ and $p(\beta_\ell|\hat{\alpha}_\ell, \hat{\alpha}_{\ell-1}, \hat{\beta}_{\ell-1}, m_1)$ is, as noted before, uniform distribution. In this case density functions of α_ℓ and β_ℓ are constant and can be omitted out of the minimization process (4.1.11). The corresponding

$g(\alpha_\ell)$ and $h(\beta_\ell)$ functions, from (4.1.6) and (4.1.7), then, are as follows.

$$g(\alpha_\ell) = -\sum_{k=(\ell-1)J+1}^{(\ell-1)J+\alpha_\ell-1} K(k), \tag{4.3.20}$$

$$h(\beta_\ell) = \sum_{k=(\ell-1)J+1}^{(\ell-1)J+\beta_\ell} K(k), \tag{4.3.21}$$

for $m_1 \leq \ell \leq m_2$. Estimates of α_ℓ and β_ℓ, can, then, be computed recursively using (4.3.20), (4.3.21), and the procedure described in section 3.8.

A comparative analysis of the above two choices of distributions (Gaussian and uniform) for α_ℓ and β_ℓ will be performed in a later section. Presently, a few examples are provided in the subsequent section to illustrate the results.

4.4 Examples

Several images have been considered to depict the results of this chapter. Figure IV.5 illustrates the "original image" versions of these pictures. Two of the original images (square and diamond) were simulated by computer. The third image (girl), was chosen to represent a natural photograph. All the images are digital with equal grid sizes of 256 by 256 picture elements. The "observable image," in each case, is obtained through determining the mean and variances of the original pictures and then adding a white Gaussian noise of specified variance (zero mean) to each picture. Figures IV.6 and

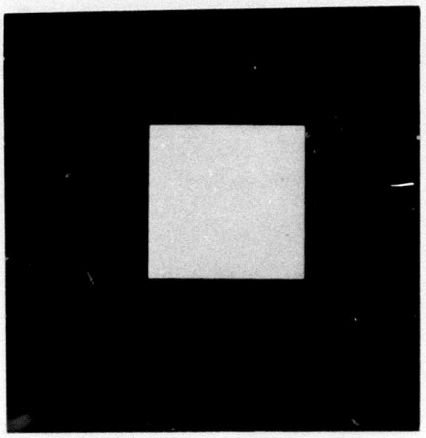

Figure IV. 5a. Original Square.

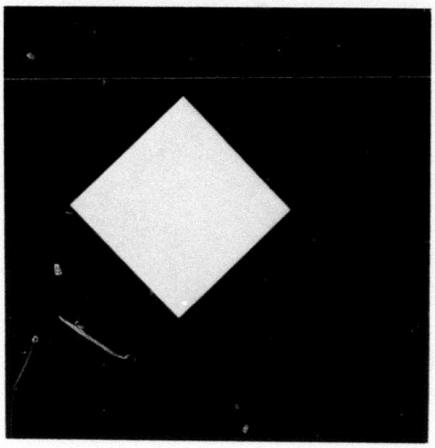

Figure IV. 5b. Original Diamond.

Figure IV. 5c. Original "Girl".

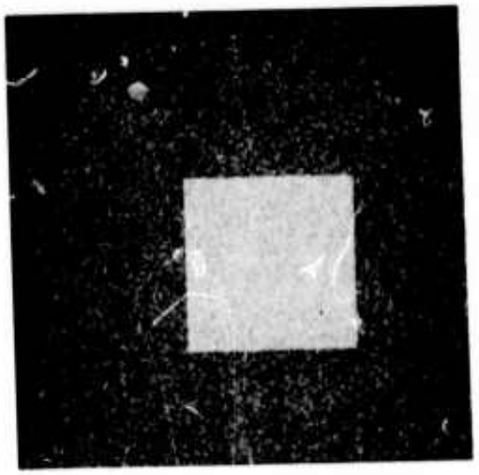

Figure IV.6a. Noisy Square
(S/N = 1.0).

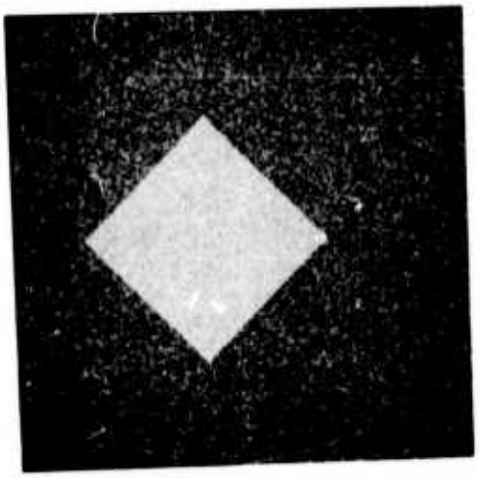

Figure IV.6b. Noisy Diamond
(S/N = 1.0).

Figure IV.6c. Noisy Girl
(S/N = 10.0).

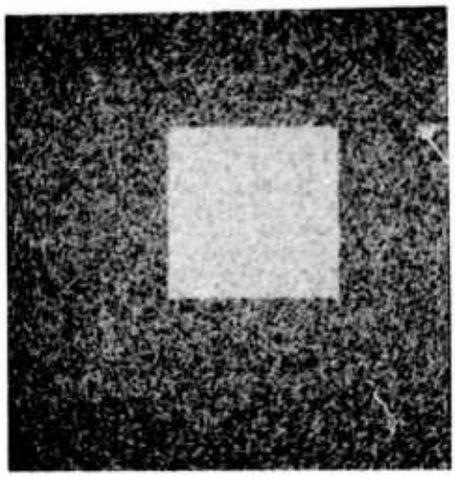

Figure IV.7a. Noisy Square (S/N = .6).

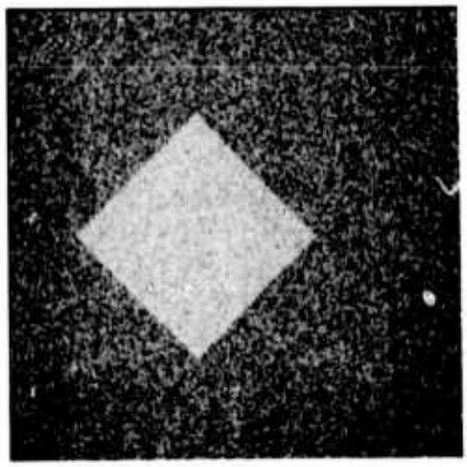

Figure IV.7b. Noisy Diamond (S/N = .6).

Figure IV.7c. Noisy Girl (S/N = .9).

IV.7 represent two sets of observable images with different signal-to-noise ratio values. An image signal-to-noise ratio, here, is defined as

$$\frac{S}{N} \triangleq \frac{\text{signal(original image) variance}}{\text{noise variance}} \tag{4.4.1}$$

An arbitrary segmentation procedure was performed to produce background, $s_b(k)$, and object, $s_0(k)$, sample functions for each image. The segmentation procedure was based on replacing the object intensity values by the maximum background grey level value (forming the background sample) and replacing the background intensity values by the minimum object grey level value (forming the object sample). In general, an estimator, as described in section 3.5, is required to perform the segmentation task. However, since the original images were available here (not usually the case), the above arbitrary technique was a more convenient procedure.

Two sets of experiments were performed reflecting results of sections 4.1 and 4.2, respectively. Statistics of α_ℓ and β_ℓ, in these experiments, were assumed Gaussian as described in section 4.3. Figures IV.8 and IV.9 illustrate outputs of the boundary estimator when values of m_1 and m_2 are given as $m_1 = 1$ and $m_2 = 256$. Note, no additional geometric information was used to delete those boundary point estimates not belonging to the object. Figures IV.10 and IV.11 depict the results of section 4.2 where locations of the first

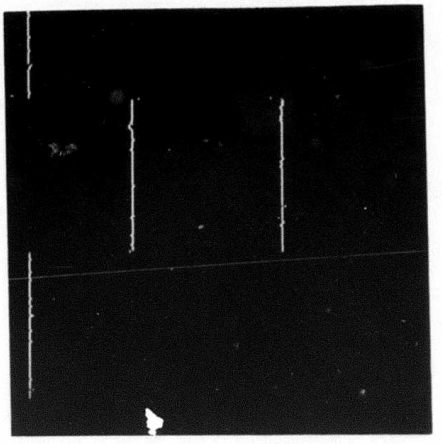

Figure IV.8a. Square Boundary.

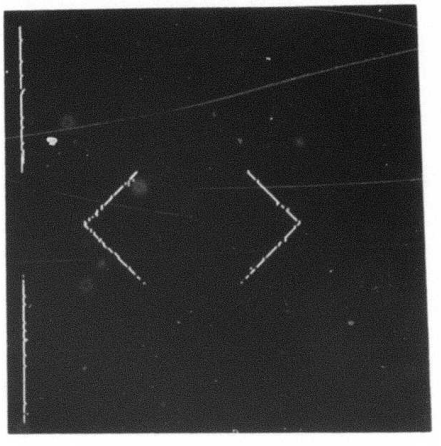

Figure IV.8b. Diamond Boundary.

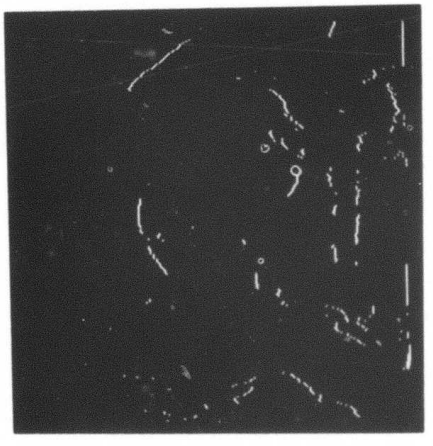

Figure IV.8c. Girl Boundary.

Figure IV.9a. Square Boundary.

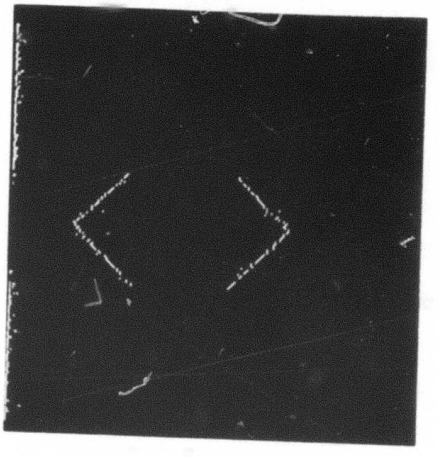

Figure IV.9b. Diamond Boundary.

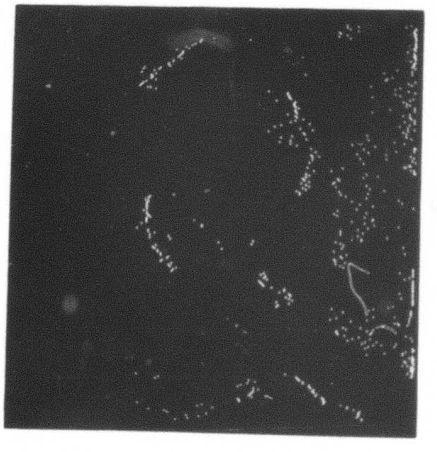

Figure IV.9c. Girl Boundary.

Figure IV.10a. Square Boundary.

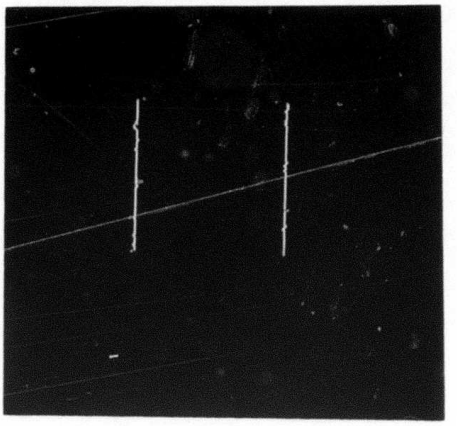

Figure IV.10b. Diamond Boundary.

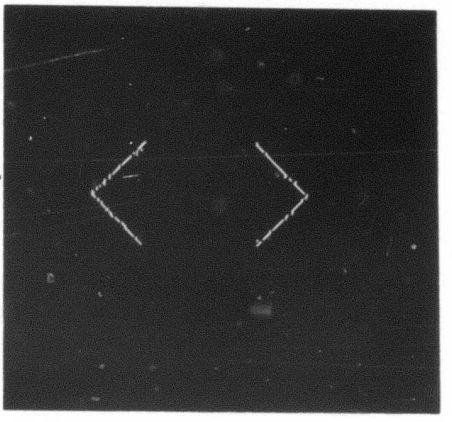

Figure IV.10c. Girl Boundary.

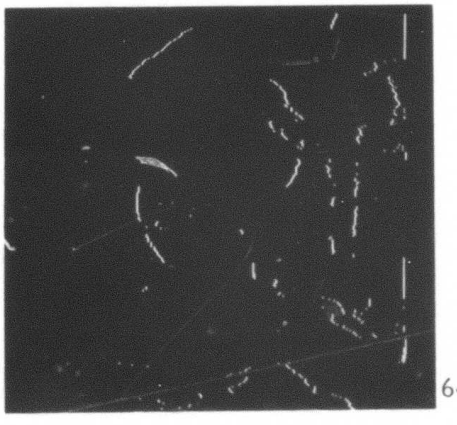

Figure IV.11a. Square Boundary.

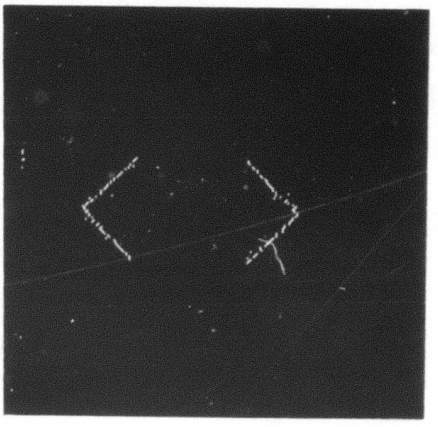

Figure IV.11b. Diamond Boundary.

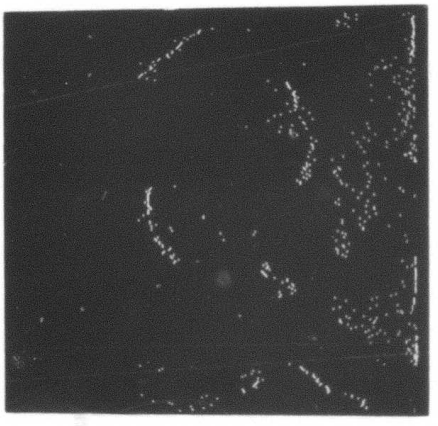

Figure IV.11c. Girl Boundary.

and last lines of the object were estimated based on statistical informations provided in section 3.4. The routine described in flow chart of Figure IV.4 was implemented to obtain estimates of m_1 and m_2. To insure that $\hat{m}_1$ and $\hat{m}_2$ represent the maximum and minimum points of the functions C(m) and Λ(m), respectively, a few lines located ahead of $\hat{m}_1$ and $\hat{m}_2$ were checked as well. The number of lines selected for this purpose are denoted by integer constants λ_{max} and λ_{min} in Figure IV.4. To keep the boundary estimator totally on-line, values of λ_{max} and λ_{min} should not exceed the quantity (m_2-m_1). For the examples illustrated here, values of λ_{max} and λ_{min}, when applicable, were chosen to be 15. No significant improvement of the results were noticed for larger values of λ_{max} and λ_{min}. Higher values of λ_{max} and λ_{min} may, however, better the results when the noise power of the image under consideration is higher than those chosen here.

Table (IV.A) summarizes the S/N ratio values of the observed images, and the conjectured values of the object maximum width, L, for each picture. Note, from relationships (4.3.3) and (4.3.9), variances of α_ℓ and β_ℓ are directly proportional to L. Various starting and ending points (α_ℓ and β_ℓ) variances were considered, by selecting different values for L, to detect the sensitivity of the boundary estimator to changes in variance values. Figures IV.9c and IV.12 are two such examples depicting the girl-boundary for

L = 250 and L = 80, respectively.

Table (IV.a)

	S/N Fig.'s (III.6, 8, 10)	S/N Fig.'s (III.7, 9, 11)	L
Square	1	.6	100
Diamond	1	.6	140
Girl	10	.9	250

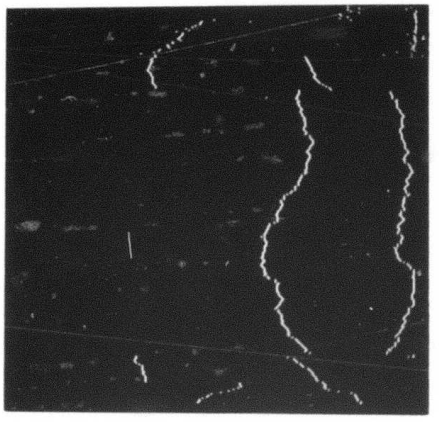

Figure IV.12. Girl Boundary for L = 80 (Compare With Fig. IV.9c where L = 250).

Chapter V

DISCUSSION AND CONCLUSION

In this chapter, we will concern ourselves with analysis of the boundary estimator. The quality of the estimator outputs, as demonstrated through examples in Chapter IV, will be discussed. Possible ways of improvement will be examined. Extensions of the estimator to multiobject images, and areas of future research will be explored.

5.1 Analysis

Referring to expression (3.6.30), i.e.,

$$(5.1.1)\qquad \min_{\underline{m},\underline{W}} \left\{ -2\sigma^2 \ln p(m_2|m_1) - 2\sigma^2 \ln p(m_1) + \sum_{\ell=m_1}^{m_2} \left[T(w_\ell) - 2\sigma^2 \ln p(w_\ell|w_{\ell-1}, m_1) \right] \right\},$$

It is evident that the boundary estimator basically capitalizes on two characteristics of the image, namely:

i) The amount of contract between the object and the background, and

ii) The statistics of the object boundary.

The contribution of the former is represented in (5.5.1) through

$$(5.1.2)\qquad \sum_{\ell=m_1}^{m_2} T(w_\ell) \ ,$$

and that of the latter is represented by

$$(5.1.3) \qquad 2\sigma^2 \ln p(m_2|m_1) + 2\sigma^2 \ln p(m_1) + 2\sigma^2 \sum_{\ell=m_1}^{m_2} \ln p(w_\ell|w_{\ell-1}, m_1).$$

Two types of statistics were chosen for the object boundary points α_ℓ and β_ℓ, namely, Gaussian and uniform. The boundary estimator designed based on the latter type of statistics, as is clear from (4.3.20) and (4.3.21), considers only the image contrast in locating the object boundary. Intuitively, then, it should be suitable for high contrast (such as binary) images.

The boundary estimator based on Gaussian statistics, on the other hand, considers both the image contrast and the boundary statistics in locating the object boundary. This is evident from (4.3.16)-(4.3.19). Varying the variances of α_ℓ and β_ℓ, in this case, one can emphasize dependence of the boundary estimator on either image contrast or object statistics. This estimator, therefore, seems to be better suited for images whose object boundaries are mostly due to textural dissimilarities rather than just contrast.

Based on the above analysis, choice of the variances of α_ℓ and β_ℓ become crucial in design of the boundary estimator based on Gaussian statistics. Locally optimum variances for α_ℓ and β_ℓ (differing from picture to picture or, in a more general setting, differing among classes of pictures), therefore, should exist. Determination of such

optimal variances, however, is not a trivial problem.

Our choice of variances as in (4.3.3) and (4.3.9), although intuitively motivated, is not claimed to be optimum. But, based on the experimental results, depicted in section 4.4, it seems to have been a suitable choice.

Since a method of selecting optimum variance values was not established, other forms of variances could result in better (or worse) estimator outputs. In fact, an alternate technique of defining the conditional variances of α_ℓ and β_ℓ will be suggested by ourselves in the next section. It will be shown, however, that this alternative definition does not always yield superior results. It is suspected, therefore, that until a consistant method of finding the optimum variances is developed, different variance values will carry different tradeoffs.

5.2 Possible Ways of Improvement

A refinement of the boundary estimator can be achieved if one believes that majority of the objects within typical images possess connected boundaries.

Recall, in section 4.3, it was assumed the conditional mean values of α_ℓ and β_ℓ are at $\hat{\alpha}_{\ell-1}$ and $\hat{\beta}_{\ell-1}$, respectively. This assumption is specially valid if the object boundary forms a connected set. However, over there, in order to not bias the boundary estimator toward connected boundaries, the variances of α_ℓ and β_ℓ were

allowed to vary freely. To capitalize on the connectiveness of the boundary, we shall restrict the magnitudes of the variances of α_ℓ and β_ℓ to be very small. Note that the flexibility of the estimator to compensate for poor estimates of α_ℓ and β_ℓ should still be one of our major concerns. In other words, utilization of connectivity property should not unduely obstruct the necessary agility of the boundary estimator. The adverse effects of such oversight will be shown by an example shortly. Note that, by utilizing the connectiveness of the object boundary, we do not expect the boundary estimator to yield a connected boundary.

A technique implemented to improve the output of the boundary estimator visually based on the connectiveness of the object boundary is described below. Let

$$\text{(5.2.1)} \qquad \mathrm{Var}(\alpha_\ell \,|\hat{\alpha}_{\ell-1}, \hat{\beta}_{\ell-1}, m_1) = \begin{cases} \sigma_\alpha^2 & \text{if } |\hat{L}_{\ell-1}-L|^2 \le C_1, \\ |\hat{L}_{\ell-1}-L|^2 & \text{if } |\hat{L}_{\ell-1}-L|^2 > C_1, \end{cases}$$

where σ_α^2 is an arbitrary small number (comparative to $|\hat{L}_{\ell-1}-L|^2$) and C_1 is an arbitrary threshold. Similarly, let

$$\text{(5.2.2)} \quad \mathrm{Var}(\beta_\ell \,|\hat{\alpha}_\ell, \hat{\alpha}_{\ell-1}, \hat{\beta}_{\ell-1}, m_1) = \begin{cases} \sigma_\beta^2 & \text{if } |\hat{L}_{\ell-1}-L|^2 \le C_2, \\ |\hat{L}_{\ell-1}-L|^2 & \text{if } |\hat{L}_{\ell-1}-L|^2 > C_2, \end{cases}$$

where σ_β^2 and C_2 are defined analogous to σ_α^2 and C_1, respectively.

Incorporation of (5.2.1) and (5.2.2) into boundary estimation algorithms described in sections 4.1 and 4.2 are easy matters. However selection of optimal values for σ_α^2, σ_β^2, and the thresholds C_1 and C_2 is not trivial.

Few examples illustrative of the effects of connectivity modification in the boundary estimation algorithm, are presented here for the sake of clarity. Figure V.1 depicts the case where

$$\sigma_\alpha^2 = \sigma_\beta^2 = .1$$

$$C_1 = C_2 = 10.$$

Notice the points forming the boundary are more centered and show less fluctuations in this figure as compared with, for example, Figure IV.8. The signal to noise ratio and other pertinent values of Figure V.1 are the same as those of Figure IV.8.

Figure V.2 has been submitted to illustrate the case where inclusion of connectivity property has overwhelmed the flexibility of the boundary estimator to a degree of losing the boundary altogether. Pertinent parameter values of this figure are identical with those of Figure IV.9.

Significant improvements in the output of the boundary estimator can be expected if one is ready to specialize the estimator further. For example, given that the objects considered will always have circular shapes, will improve the final results considerably.

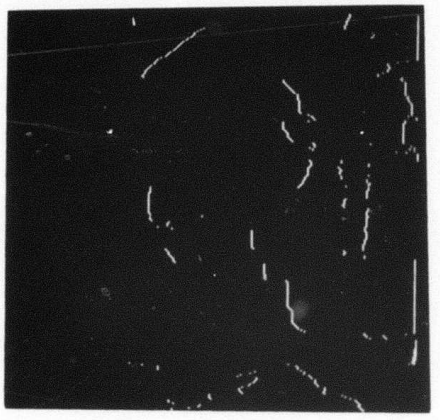

Figure V.1. Effect of Connectivity on the "Girl" Boundary.

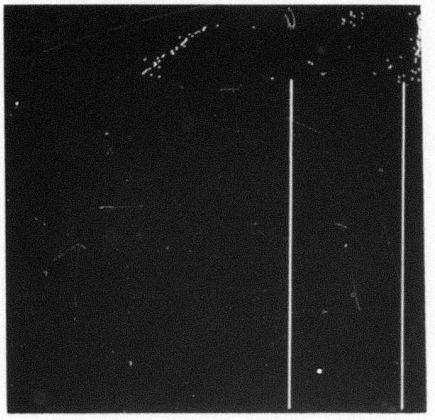

Figure V.2. Adverse Effect of Connectivity on the "Girl" Boundary.

Availability of such informations, however, cannot be visualized as practical if one is to develop generally applicable boundary estimators.

5.3 Extensions of the Estimator to Multiobject Images

As mentioned in section 5.1, the boundary estimator basically capitalizes on two characteristics of the image, namely, the amount of object-background contract and the statistics of object boundary. The contrast is an inherent property of the image. The statistics, however, can be manipulated to improve the results. For the Gaussian statistics chosen in this work, the variances of α_ℓ and β_ℓ were arbitrary. A small variance would instruct the boundary estimator to emphasize its dependence on the statistics of the object boundary, whereas, a large variance would encourage the estimator to rely mainly on the amount of contract between the object and background. This dichotomy of the boundary estimator suggests a method of obtaining boundaries for multi-object images.

Assuming the variances of α_ℓ and β_ℓ are suitably defined, for example as in (4.3.3) and (4.3.9), for each object in a multi-object image, a classification of the objects is made based on their maximum size. This is possible since the variances are directly proportional to the objects maximum sizes. The boundary estimator is then biased to look for an object with maximum size L_i, where i denotes the $i^{\underline{th}}$ object. Once this object is located (its boundary determined), its detail, represented by the $i^{\underline{th}}$ object sample function,

is replaced by the background sample function. The procedure is then repeated until the boundary of the last object is determined.

The above suggested technique is based on the replacement processing concept delineated previously. It is mainly suitable for images with nonoverlapping objects. Furthermore, the segmentation procedure required to determine various objects and background sample functions is a crucial operation here and it should be performed based on techniques described in section 3.5.

As a by product of considering multi-object images, we observe that the optimum variance functions of α_ℓ and β_ℓ should depend on some characteristic of the object in the image so as to differentiate it from other objects. This is another readon, not possible to explain until now, that we defined the variances of α_ℓ and β_ℓ as functions of the object maximum width in (4.3.3) and (4.3.9).

Suitability and verification of the above suggested procedure to obtain boundaries of multi-object images is left as a future research topic. Other topics meriting further research are discussed in the following section.

5.4 Areas of Future Research

Digital image processing techniques, as opposed to analog (optical) techniques, are generally based on utilization of digital computers. As a result, development of efficient computational algorithms, aimed at alleviating the amount of time and storage

required to process an image, have been given special attention in the literature [5-7]. Recursive computational procedures, usually, retain the above mentioned desired features for implementation on a computer.

The proposed recursive solution of the minimization process (3.6.30), delineated in Chapter IV, was an attempt to produce a computationally efficient algorithm for the boundary estimator. Forcing a recursive solution on (3.6.30), however, may have affected the results adversely. Although satisfactory experimental results favored the recursive solution, implementation of parallel computers, for processing the minimization (3.6.30), could clearly yield improved estimates of the boundary. An efficient algorithm applicable to computers with parallel processing capabilities, therefore, should be considered in the future when such computers are readily available.

Accepting utilization of sequential computers as the most efficient choice at present, and furthermore, the Gaussian statistics as reasonable choice of density functions for α_ℓ and β_ℓ, development of a method to determine optimum variance values for α_ℓ and β_ℓ is another area meriting further research.

Appropriate extensions of the boundary estimator to multi-object images is another interesting problem. An intuitively justified procedure, based on available geometric information about

the objects within the image (such as their maximum sizes) was described in section 5.3. Development of a boundary estimator based on the replacement processing concept is, however, a more direct approach to derive a multi-object boundary estimator. Such a procedure would require explicit representation of γ_i's, defined in section 2.7, in terms of the boundary points of each object. Further work to explore the possibilities of such representations for γ_i's seems, henceforth, to be worthwhile.

5.5 Conclusion

The feasibility of resolving boundary determination problems through existing estimation concepts was established. An implementable boundary estimator, based on a combination of deterministic and probabilistic information pertaining to the image, was developed and its performance was satisfactorily tested through a few examples. The boundary estimator was designed to be recursive, hence, making it computationally attractive. The recursive processing of images is specially desirable because of the enormous amount of data and computations involved. Finally, although the boundary determination procedure developed in this work is not claimed to be superior to other existing techniques in all cases, its methodological formulation is hoped to generate further interest and insight into design of future boundary determination techniques.

REFERENCES

[1] Huble, D. and Weisel, W., J. Neurophysiol. March 1965, No. 2, Vol. 1 XXVIII, page 287.

[2] Yarbus, A. L., Eye Movements and Vision, Translation Editor: Lorin A. Riggs (Russian) (Plenum Press, New York, 1967).

[3] Thomson, W. B., "The Role of Texture in Computerized Scene Analysis," USCIPI Report 550, December 1974.

[4] Franks, L. E., "A Model for the Random Video Process," Bell Syst. Tech. J., April 1966.

[5] Nahi, N., and Assefi, T., "Bayesian Recursive Image Estimation," IEEE Trans. on Computers, Vol. C-21, No. 7, July 1972.

[6] Habibi, A., "Two Dimensional Bayesian Estimate of Images," Proceedings of the IEEE, Vol. 60, No. 7, July 1972.

[7] Nahi, N., and Franco, C. , "Recursive Image Enhancement Vector Processing," IEEE Trans. Communications, Vol. 60, No. 7, July 1972, pp. 872-877.

[8] Duda, R., and Hart, P. , Pattern Classification and Scene Analysis, John Wiley and Sons, Inc., New York, 1973.

[9] Lipkin, B., and Rosenfeld, A., Picture Processing and Psychopictorics, Academic Press, New York, 1970.

[10] Prewitt, J. M. S., "Object Enhancement and Extraction," Picture Processing and Psychopictorics, Academic Press, 1970.

[11] Rosenfeld, A., "A Nonlinear Edge Detection Technique," Proceedings of the IEEE, May 1970, Letters, Vol. 58, No. 5.

[12] Argyle, E., "Techniques for Edge Detection," Proceedings of the IEEE, Feb. 1971, Vol. 59, No. 2.

[13] Goodman, A. W., Analytic Geometry and the Calculus, Macmillan Company, New York, 1963.

[14] Greanias, E. , Meagher, P., Norman, R., and Eissinger, P., "The Recognition of Handwritten Numerals by Contour Analysis," IBM Journal, 7, January 1963.

REFERENCES (Cont'd)

[15] Rosenfeld, A., "Connectivity in Digital Pictures," J. ACM, 17, Jan. 1970.

[16] Zahn, C. T., "A Formal Description for Two-Dimensional Patterns," Proc. Int. Joint Conf. on Art. Int., D. E. Walker, and L. M. Norton, eds., May 1969.

[17] Pingle, K. K., "Visual Perception by a Computer," in Automatic Interpretation and Classification of Images, A. Grasselli, ed., Academic Press, New York, 1969.

[18] Kelly, M. D., "Edge Detection in Pictures by Computer Using Planning," in Machine Intelligence 6, B. Meltzer and D. Michie, eds., American Elsevier Publishing Co., New York, 1971.

[19] Rosenfeld, A., Picture Processing by Computer, Academic Press, New York, 1969.

[20] Rosenfeld, A., and Troy, E., "Visual Texture Analysis," Univ. of Maryland, College Park, Technical Report 182-2, Nov. 1971.

[21] Nahi, N. E., "Detection of Objects in Noisy Pictures," USCEE Report 425, March 1972-August 1972.

[22] Franks. L., Signal Theory, Prentice-Hall, Inc., Englewood Cliffs, N.J., 1969.

[23] Nahi, N. E., "Role of Recursive Estimation in Statistical Image Enhancement," Proc. of the IEEE, Vol. 50, No. 7, July, 1972.

[24] Nahi, N. E., Estimation Theory and Applications, Wiley, New York, 1969.

[25] Franco, C. A., "Recursive Image Estimation," Ph.D. Dissertation, Dept. of Electrical Engineering, Univ. of Southern Calif., Los Angeles, Feb. 1973.

[26] Papoulis, A., Probability, Random Variables, and Stochastic Processes, McGraw-Hill, N.Y., 1965.

[27] Pratt, W. K., Digital Image Processing, to be published.

BIBLIOGRAPHY

[1] Rosenfeld, A., Thurston, M., Lee, Y. H., "Edge and Curve Detection: Further Experiments," Special Issue on Two Dimensional Digital Signal Processing, pp. 677-715, July 1972.

[2] Schreiber, W. F., Huang, T. S., Tretiak, O. J., "Contour Coding of Images," Proceedings of the Picture Bandwidth Compression Symposium, Gordon and Breach, New York, Part 3, December 1971.

[3] Sitton, G. A., Tobias, P. R., "Applications of the Laplacian to Image Processing," IBM Publication No. 320.2410, February 1, 1971.

[4] Argyle, E., "Techniques for Edge Detection," Proceedings of the IEEE, Vol. 59, No. 2, pp. 235-287, February 1971.

[5] Diamantides, N. D., "Correlation Measure of Contrast for MAP Matching," Journal of the Optical Society of America, Vol. 58, No. 7, July 1968, pp. 996-998.

[6] Diamantides, N. D., "Gaussian Pictorial Fields and Their Definition by Means of a Correlator," Applied Optics, Vol. 8, No. 4, April 1969, p. 818.

[7] Donaldson, R. W., Toussoint, G. T., "Use of Contextural Constraints in Recognition of Contour-Traced Handprinted Characters," IEEE Transactions on Computers, Vol. C-20, No. 8, p. 1096, August 1971.

[8] Gattis, J. L., Wintz, P. A., "Automated Techniques for Data Analysis and Transmission," Purdue University, School of Electrical Engineering, NGR-15-005-106, TR-EE 71-37, Lafayette, Indiana, August, 1971.

[9] Gouriet, G. G., "A Method of Measuring Television Picture Detail," Electronic Engineering, Vol. 24, July, 1952, pp. 308-311.

[10] Krakauer, L. J., "Computer Analysis of Visual Properties of Curved Objects," MAC TR-82, MIT, Cambridge, Massachusetts, May 1971.

BIBLIOGRAPHY (Cont'd)

[11] Deutsch, E. S., Belknap, N. J., "Texture Descriptors Using Neighborhood Information," Computer Graphics and Image Processing, Vol. 1, No. 2, pp. 145-168, August 1972.

[12] Haralick, R. M., Shanmugam, K., Dinstein, I., "On Some Quickly Computable Features for Texture," Proceedings of the Symposium on Computer Image Processing and Recognition, Paper No. 12-2, Columbia, Missouri, August 1972.

[13] Ledley, R. S., "Texture Problems in Biomedical Pattern Recognition," Proceedings of the 1972 IEEE Conference on Decision and Control and 11th Symposium on Adaptive Processes, Library of Congress Catalog #TJ217,117,1972, New Orleans, Louisiana, pp. 590-595, December 13-15, 1972.

[14] Pickett, R. M., "Perceiving Visual Texture - A Literature Survey," Harvard University, Cambridge, Massachusetts, Final Report, August 1964 - August 1966, Wright-Patterson Air Force Base, Ohio, AMRL-TR-68-12, March 1968.

[15] Read, J. S., Jayaramamurthy, S. N., "Automatic Generation of Texture Feature Detectors," IEEE Transactions on Computers, Vol. C-21, No. 7, pp. 803-811, July 1972.

[16] Sutton, P. N., Hall, E. L., "Texture Measures for Automatic Classification of Pulmonary Disease," IEEE Transactions on Computers, Vol. C-21, No. 7, pp. 667-676, July 1972.

[17] Tamches, I., "On Texture Representation and Filtering," Proceedings of the Symposium on Computer Image Processing and Recognition, Paper No. 12-1, Columbia, Missouri, August, 1972.

[18] Kruger, R. P., Dwyer, S. J., "Computer-Aided Diagnosis of Radiographic Cardiac Size and Shape Descriptors," Proceedings of the Third Annual Houston Conference on Computer and System Science, University of Houston, Houston, Texas, April 26-27, 1971.

[19] Kruger, R. P., Harlow, C. A., Dwyer, S. J., "Automated Diagnosis Utilizing Cardiac Size and Shape Descriptors," Proceedings of the Fifth Annual Princeton Conference on Information Sciences and Systems, Princeton, New Jersey, March 25-26, 1971.

[20] Kruger, R. P., Townes, J. R., Hall, D. L., Dwyer, S. J., "Computer Aided Diagnosis Via Feature Extraction and Classification of Radiographic Cardiac Size and Shape Descriptors," Ninth Annual Symposium on Biomathematics and Computer Science in the Life Sciences Proceedings, Houston, Texas, March 22-24, 1971.

[21] Kubra, M. H., "Automatic Picture Detail Detection in the Presence of Random Noise," Proceedings of the IEEE, Vol. 51, No. 11, November 1963, pp. 1518-1523.

[22] Kubra, M. H., "Methods of Measuring Picture Detail in Relation to Television Signal Bandwidth Compression," University of London, Ph.D. Thesis, 1962.

[23] Langridge, D. J., "On the Computation of Shape," Frontiers of Pattern Recognition, Academic Press, pp. 247-365, New York, 1972.

[24] MacLeod, I. D. G., Argyle, E., "Comments on 'Techniques for Edge Detection,'" Proceedings of the IEEE, Vol. 60, No. 3, p. 344, March 1972.

[25] Martelli, A., "Edge Detection Using Heuristic Search Methods," Computer Graphics and Image Processing, Vol. 1, No. 2, pp. 169-182, August 1972.

[26] Maxwell, P. C., "The Perception and Description of Line Drawings by Computer," Computer Graphics and Image Processing, Vol. 1, pp. 31-46, April 1972.

[27] Orton, J. N., Rosenfeld, A., "Two Programs for Delineating 'Solid' and 'Broken' Regions in an Image," Computer Science Center, Marylard University, College Park, January 1965.

[28] Pfaltz, J. L., Rosenfeld, A., "Computer Representation of Planar Regions by Their Skeletons," Association of Computing Machinery, Vol. 10, pp. 118-125, February 1967.

[29] Richard, C. W., Hemani, H., "Identification of Three-Dimensional Objects Using Fourier Descriptors of the Boundary Curve," Proceedings of the Symposium on Computer Image Processing and Recognition, Paper No. 15-2, Columbia, Missouri, August, 1972.

[30] Rosenfeld, A., "A Nonlinear Edge Detection Technique," Proceedings of the IEEE, Letters, Vol. 58, No. 5, pp. 814-816, May 1970.

[31] Rosenfeld, A., Thurston, M., "Edge and Curve Detection for Visual Scene Analysis," ARCRL-70-0488, Computer Science Center, University of Maryland, GSFC Technical Report No. 70-128, August 1970.

[32] Rosenfeld, A., Thurston, M., "Edge and Curve Detection for Visual Scene Analysis," IEEE Transactions on Computers, Vol. C-20, No. 5, pp. 562-569, May 1971.